9-1-2022

Developing Scaling Laws to Predict Compressive Mechanical Properties and Determine Geometrical Parameters of Modified BCC Lattice Structures

Hasanain S. Abdulhadi

Abdalsalam Fadeel
Wright State University, fadeel.2@wright.edu

Tahseen A. Alwattar

Ahsan Mian
Wright State University - Main Campus, ahsan.mian@wright.edu

Received: 8 March 2022 | Revised: 14 July 2022 | Accepted: 8 August 2022

DOI: 10.1002/eng2.12566

RESEARCH ARTICLE

Engineering Reports Open Access WILEY

Developing scaling laws to predict compressive mechanical properties and determine geometrical parameters of modified BCC lattice structures

Hasanain S. Abdulhadi | **Abdalsalam Fadeel** | **Tahseen A. Alwattar** | **Ahsan Mian**

Department of Mechanical and Material Engineering, Wright State University, Dayton, Ohio, USA

Correspondence
Ahsan Mian, Department of Mechanical and Material Engineering, Wright State University, 3640 Colonel Glenn Hwy., Dayton, OH 45435, USA.
Email: ahsan.mian@wright.edu

Abstract

The objective of this study is to develop generalized empirical closed-form equations to predict the compressive mechanical properties and determine geometrical parameters. To achieve that, 117 models are built and analyzed using ABAQUS/CAE 2016 to provide two types of reliable data: one for lattice mechanical properties based on finite element method and the other for geometrical parameters using the measurements of ABAQUS diagnostic tool. All the models are created by modifying the basic feature of body-centered cubic lattice structure based on a range of strut angles, a set of relative densities, and two design sets. Also, the influence of lattice cell tessellations and material distribution at strut intersections are considered within these models to provide accurate results. The first data set is fitted with the scaling laws, relating relative elastic modulus and stress with the relative density, to determine Gibson and Ashby's coefficients. The second type of data regarding lattice geometries is correlated with the relative density to estimate actual lattice volume, strut radius, aspect ratio, and overall lattice volume. By this way, these equations can be used to predict directly the lattice characteristics and geometrical parameters without the need for ABAQUS. The results show that the generalized empirical closed-form equations can predict well both the lattice characteristics and geometries. In addition, the relative stresses and elastic modulus increase with increasing the strut angles since the main deformation mechanisms move toward stretch-dominated rather than bending. Besides, Gibson and Ashby's coefficients along with the geometrical factors of aspect ratios are found to be approximately similar for both generations. This study contributes to developing efficient equations to provide the researchers with a preliminary insight about the best lattice design and its compatibility in a certain application before starting the fabrication process.

KEYWORDS

compressive mechanical properties, finite element method, geometrical parameters, modified BCC lattice structures, scaling Laws

JEL CLASSIFICATION

Mechanical engineering

1 | INTRODUCTION

Lattice structure (LS) is defined as an interconnected array of solid struts or assembly of multiple micro-trusses. It is recognized as a periodic architecture, comprising of unit cells of the same shape and size placed at equal distances in the principal directions. The periodic LSs exhibit better mechanical properties (for example, the specific stiffness and strength) than those offered by traditional foams, which are considered good candidates for the energy-absorption applications. The foams belong to the category of stochastic cellular materials,[1,2] and have irregular cell structures in which unit cells of different shapes or sizes are distributed randomly. The irregularity in the microstructure of the foam materials induces localized damage at the point of weakness, leading to an overly conservative design.[3,4] While, the regular distribution of the unit cells enables adjusting the mechanical properties of LSs. Thus, the periodic materials, LSs, are generally preferable than the stochastic ones, foam materials. As such, they have attracted much attention in recent studies, and become a good candidate in various applications, including biomedical science, aerospace engineering, and vibration isolation.[5]

Previously, the design field of periodic cellular materials was limited to using two-dimensional channels, namely, prismatic materials for instance honeycomb. This limitation is traced back to the difficulty of manufacturing complex geometries using conventional manufacturing methods. While in recent years, the emergence of additive manufacturing technology facilitates the fabricating process of 3D complex parts and makes it simple compared to the traditional methods. The variety in the designs of LSs, accompanied by controllability of the pore size and shape along with manufacturability at a good level of accuracy, is attributed to the advancement of additive manufacturing (AM) or 3D printing.[6–9] This in turn stimulates the field of lattice design to grow and expand broadly in order to meet the needs of many applications, not only because of their lightweight, but also due to their interesting mechanical characteristics.

The mechanical characteristics of cellular materials are dependent on the solid constitutive material properties, the topology of the lattice, and relative density (RD).[10,11,12,13] It is defined as the ratio of actual lattice material volume to the overall block volume that encloses the lattice ($RD = V_{latt.}/V_{sol.}$). Similarly, RD is also defined as the ratio of the lattice density to the corresponding one of solid block enclosing the lattice ($RD = \rho_{latt.}/\rho_{sol.}$). In essence, holes, voids, or pore sizes of the cellular materials are reduced with increasing RD, resulting in higher mechanical properties. Besides, the deformation mode of the cellular materials whether bending- or stretch-dominated relies mainly on the lattice topology, which has a major influence on the mechanical response of cellular materials.[14] Significantly, the coupled effects of RD and lattice topology on the mechanical response of the cellular materials have been formulated into a set of useful relationships introduced by Gibson and Ashby.[10,11] The one that correlates the relative elastic modulus (RE) with the RD, that is, $RE = c_1 RD^n$, has attracted much attention in the earlier studies, and there is another correlation for the relative stress (RS) with RD, namely, $RS = c_5 RD^m$. Here, RE is defined as the ratio of equivalent lattice modulus to solid constitutive material modulus ($RE = E_{latt.}/E_{Sol.}$) and RS is the ratio of the equivalent yield stress of lattice to yield stress of solid constitutive material ($RS = Y_{latt.}/Y_{Sol.}$). Also, c_1, c_5, and n, m are called Gibson and Ashby's coefficients and exponents, respectively. It has been found that the exponent (n) depends on the lattice topology such that it has approximately a value of 1 for stretch-dominated cellular materials whose cell structures resist tension or compression.[1,12,15,16] Also, it can have roughly a value of 2 for cellular materials with bending-dominated topologies in which cell walls undergo bending.[10–12] Thus, the stretch-dominated cellular materials at a certain value of RD exhibit extraordinary stiffness, whereas; the bending-dominated ones corresponding to the same RD are more complaint.[1,10,11,15,16] In addition, Maskery et al.[17] and Ahmadi et al.[18] proved that the scaling exponent (n) can have values less than 1, between 1 and 2, or greater than 2, based on various lattice cell configurations. Furthermore, Ahmadi et al.[18] classified a set of LSs based on the scaling exponent (n): $n \leq 1.5$ for stiff structures, and $n > 1.5$ for compliance ones. In this regard, the other scaling exponent (m) can have a value of 1.5 for bending-dominated structures and 1 for stretch-dominated ones.[19] In addition, the values of m can be within a range of 1 to 2 or higher than 2 based on the geometrical shape of lattice unit cells.[18]

The scaling relationship between the RE and RD plays a crucial role in designing the cellular materials. This is due to the possibility of tailoring the elastic modulus directly by adjusting the RD. For that purpose, the scaling constants (n and c_1) should be determined based on the power curve fitting of the measured data. Also, the scaling law relating RS with RD is of high importance in identifying the failure limit of the lattice. The associated coefficients (m and c_5) can be estimated in a similar way to the former scaling constants. Likewise, the yield stress can also be manipulated by changing RD.

Significantly, the scaling laws are efficient techniques not only for analyzing lattice behavior based on deformation modes but also for predicting elastic modulus and yield stress. This could be much better than the experimental work, analytical solution, or finite element method (FEM), especially when thinking about saving human time and effort.

Typically, fabricating the lattice specimens and conducting experimental tests on them usually require a longer time and higher cost.[18,20–25] In addition, the traditional analytical approaches to predicting the mechanical behavior of the lattice are not without limitations. The most significant one is the inaccurate measurement of the actual lattice volume due to not considering the material overlapping at the strut joints.[26,27] In addition, neglecting the effect of deformation induced by the shear loadings renders them applicable only to LSs of small RDs.[26] Also, most of the analytical methods are commonly created to be appropriate for single lattice unit cells with equal dimensions.[26,28] Besides, the mechanical behavior of LSs with the higher number of unit cells cannot be captured accurately from the behavior of single-unit cells. For this reason, homogenization is needed when working on single-unit cells to predict the mechanical characteristics of LSs with the higher number of unit cells.[27,29] To this end, many researchers dedicated FE models to predicting the mechanical properties of LSs. However, these models were limited to specific lattice configurations of equal dimensions, for instance, body-centered cubic (BCC), reinforced BCC, triply periodic minimal surfaces (TPMS), cube, face diagonal cube, octahedron, octet, void octet, truncated cube, and truncated octahedron.[16,17,25,29,30]

It is also worthwhile explaining the most recent studies about the multi-scale design and optimization methods, as well as the strategies of modeling the lattice structures. Bertolino and Montemurro[31] applied a topological optimization of two scales on anisotropic cellular material for a single unit cell representing the microscale level and entire lattice considered as macroscale level under nonzero Neumann–Dirichlet boundary conditions. In this regard, a multi-scale topology optimization method for lattices was introduced by Reference 32, including a description for a representative volume element based on the nonuniform rational basis spline hyper-surfaces, solid isotropic material with penalisation approach, and homogenization method using strain energy to conduct the scale transition. In addition, a general multi-scale optimization method was used to design lattice materials subjected to boundary conditions of various nature (i.e., geometric, manufacturing, and thermodynamic constraints) and different scales. The geometric and manufacturing constraints are considered at mesoscopic scale, while the thermodynamic constraints are regarded within macroscopic scale. The main goal of this method is to apply a surface optimization for the representative volume element of a lattice, comprising both the local and global geometric parameters of the surface.[33] To this end, a gradient lattice structure was designed using computer-added design-compatible topology optimization method based on spline hyper-surfaces and solid isotropic material with penalization approaches. This study was conducted to evaluate the effective thermal conductivity of periodic cellular materials starting with 31 various configurations. After that, seven configurations were selected to design the gradient lattice feature with the help of optimization method. In general, the effective thermal conductivity was found to be dependent on the relative density and the lattice topology.[34]

In the current research, the elastic–plastic compressive mechanical behavior and the structural parameters of modified BCC LSs are investigated based on FEM and scaling law analysis in order to create generalized empirical closed-form equations for the purpose of accurately and efficiently predicting the compressive mechanical properties (CMPs) and determining the geometrical parameters (GPs) by including the effect of lattice cell tessellation and material distribution at strut joints. To achieve that goal, the following steps as the main strategy of this work are carried out:

1. Thirteen models of modified BCC LSs with $3 \times 3 \times 3$ cells having the same strut diameters are adopted here.
2. These models are categorized based on strut length into two sets, fixed and varied strut length models, referred to here as FSLMs and VSLMs, respectively. Each one comprises seven models corresponding to strut angle variation from 40° to 100° with a step of 10°.In the first set, the strut length as a design constraint is kept fixed with strut angle variation. While in the second set, it is varied from one model to another with strut angle variation. The lattice model with 70.53° strut angle is selected as a reference model denoted by RM. This model represents the basic configuration of BCC LS with equal dimensions, $15\,\text{mm} \times 15\,\text{mm} \times 15\,\text{mm}$ in x, y, and z directions. Due to the repetition of the RM in both sets, the number of modified BCC lattice models created initially is 13. In this respect, the experimental work will be conducted on the reference model for the purpose of validating the boundary and loading conditions.
3. Corresponding to each one of the 13 models, other nine lattice models of different RDs within a range from 0.14 to 0.3 with a step of 0.02 are created by changing the strut diameters. As such, the total number of models adopted in the current research is 117.
4. Elastic–plastic FE simulation of the quasi-static axial compression behavior is conducted for all lattice models using ABAQUS FE software to find the CMPs. In addition, ABAQUS diagnostic tools are used to measure accurately the GPs of all adopted models.

5. The data extracted from ABAQUS are fitted with Gibson and Ashby's scaling laws and correlated with RDs to find Gibson and Ashby's constants and the other geometrical factors, thereby creating five main empirical closed-form equations. Two of them relate RE and RS with RD, and the others correlate the actual lattice volume, strut radius and aspect ratio with RD.
6. Validation of these equations is achieved by comparing their results with those of ABAQUS FE software, showing a good agreement in the results between them. In the meanwhile, prediction results of GPs based on the empirical equations are proved to be more accurate than those of the traditional geometrical equations. This is mainly due to considering the effect of material overlapping at strut junctions when creating the empirical equations and ignoring that effect in the formulation of the traditional equations.
7. The influence of lattice cell tessellation is also considered when developing the empirical closed-form equations in order to generalize them. By this way. The prediction range of CMPs will be expanded to cover the elastic modulus, yield stress, and the associated mechanical characteristics for $\geq 3 \times 3 \times 3$ unit cells. In addition, the prediction capacity of the GPs is extended to comprise the actual lattice volume, strut radius, aspect ratio, strut length, and the overall lattice solid volume for $\geq 1 \times 1 \times 1$ unit cells.
8. In essence, the generalized empirical-closed form equations developed in the current research provide lattice designers swift and thorough insight into the elastic–plastic compressive mechanical behavior and structural parameters of a wider range of BCC LSs before starting the fabrication process or conducting FE simulation, thereby saving more time, effort, and expenses.

The outline of this article starts with an experimental work about fabricating the lattice samples and testing their mechanical response under compressive loading. Hence, the design features of all lattice models adopted in the current research are explained. Then, finite element modeling is discussed with an emphasis on the mechanical properties of material forming the lattice struts, boundary and loading conditions, and effective lattice modulus and yield strength. After that, meshing the lattice models with using hexahedron elements is illustrated. In addition, mesh convergence analyzes and the influence of lattice cell tessellation are investigated for the adopted lattice models. Up to this point, the results of the finite element models and experimental work are discussed, and a validation of the closed-form equations is performed. The final section of this manuscript includes a short summary and conclusion of the current study as well as a future work.

2 | EXPERIMENTAL WORK

The experimental work utilized in the current investigation is to validate the boundary and loading conditions adopted for the finite element models. First, the reference model was designed with the help of smart procedure using ABAQUS software, then saved in standard tessellation language (STL) format, and exported to the 3D-printer software, CatalystEX. Next, three specimens of the reference model were printed on a fused deposition modeling (FDM) based 3D printer uPrint-SE-Plus provided by Stratasys. In this regard, the default processing parameters (0.254 mm layer thickness and high sparse density) were selected to print these specimens. Furthermore, the printing chamber and head temperatures were about 70 and 300°C, respectively. In addition, the material used to fabricate the specimens was acrylonitrile butadiene styrene (ABSplus-P430), which is a thermoplastic material. After completing the printing process, the specimens need to be washed using Stratasys cleaning apparatus (SCA), 1200HT, to remove the support material. As shown in Figure 1, the compression test was conducted on three samples to confirm the repeatability using a mechanical testing machine called TESTRESOURCES with a load capacity and displacement rate of 250 lbf and 0.5 mm/min, respectively.

3 | GENERATING THE OVERALL LATTICE MODELS

The structural design of the lattice adopted in the current research is a modified version of the BCC lattice configuration based on strut length and orientation. As mentioned earlier, 13 lattice models were divided as FSLMs and VSLMs, each with strut angle variations from 40° to 100° with a step of 10°. As part of the structural design of FSLMs, the strut length is kept fixed through the layers of a certain model and for all seven models with varying strut angles. To achieve that, both the square base area and the height are manipulated from one model to another as shown in Figure 2A. To explain that, the height increases and the base area decreases with increasing the strut angles and vice versa. On the other

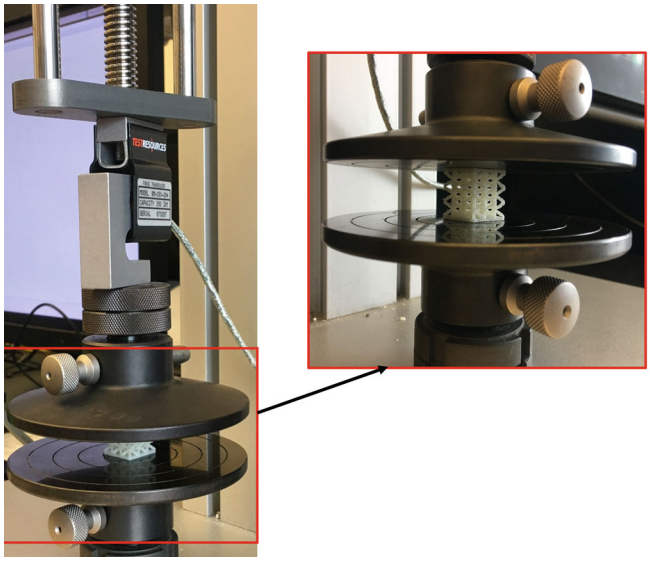

FIGURE 1 A mechanical testing machine used to apply a compressive loading on the 3D-printed lattice

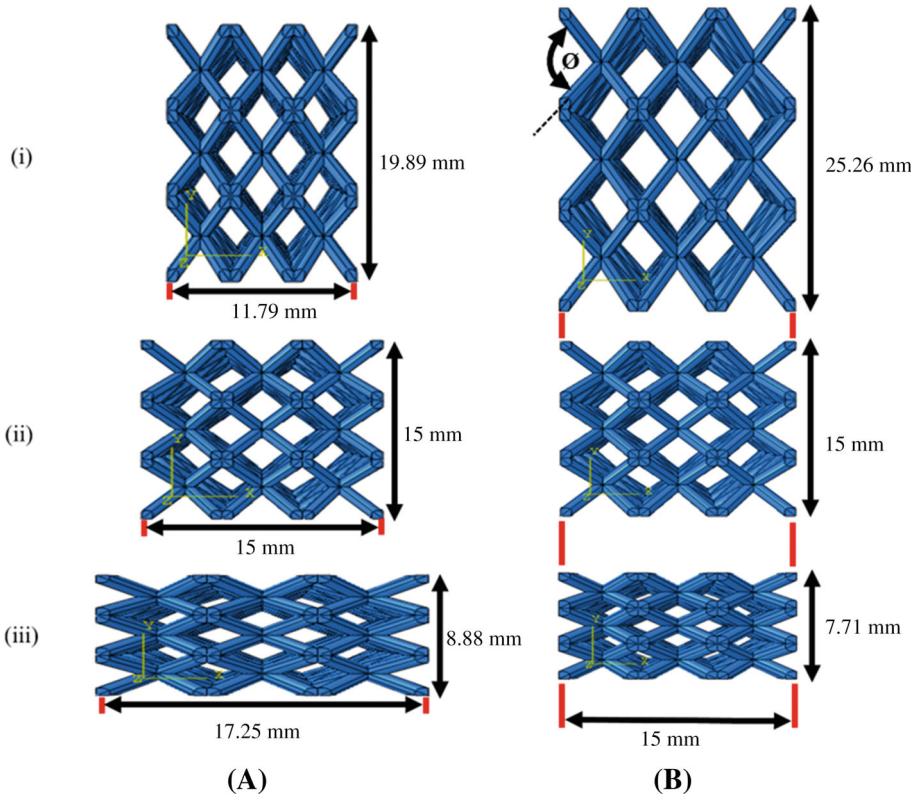

FIGURE 2 The structural design of (A) FSLMs and (B) VSLMs for (i) Ø = 100°, (ii) Ø = 70.53° and (iii) Ø = 40°

side in the design of VSLMs, the square base area of a single unit cell or an entire lattice is kept the same through one model and for all other seven models with changing the strut angles, but the height increases with increasing the strut angles as shown in Figure 2B. Therefore, the strut length also increases with increasing the strut angles. This means, the strut length is fixed through the layers of the same model but varied from one model to another with strut angle variation.

The next step after introducing the LS design is to create additional models of various RDs corresponding to each one of the 13 modified BCC lattice models. For that purpose, a range of RDs from 0.14 to 0.3 with the step of 0.02 is set as a target to build nine lattice models based on varying the strut radius. In other words, a parametric study was

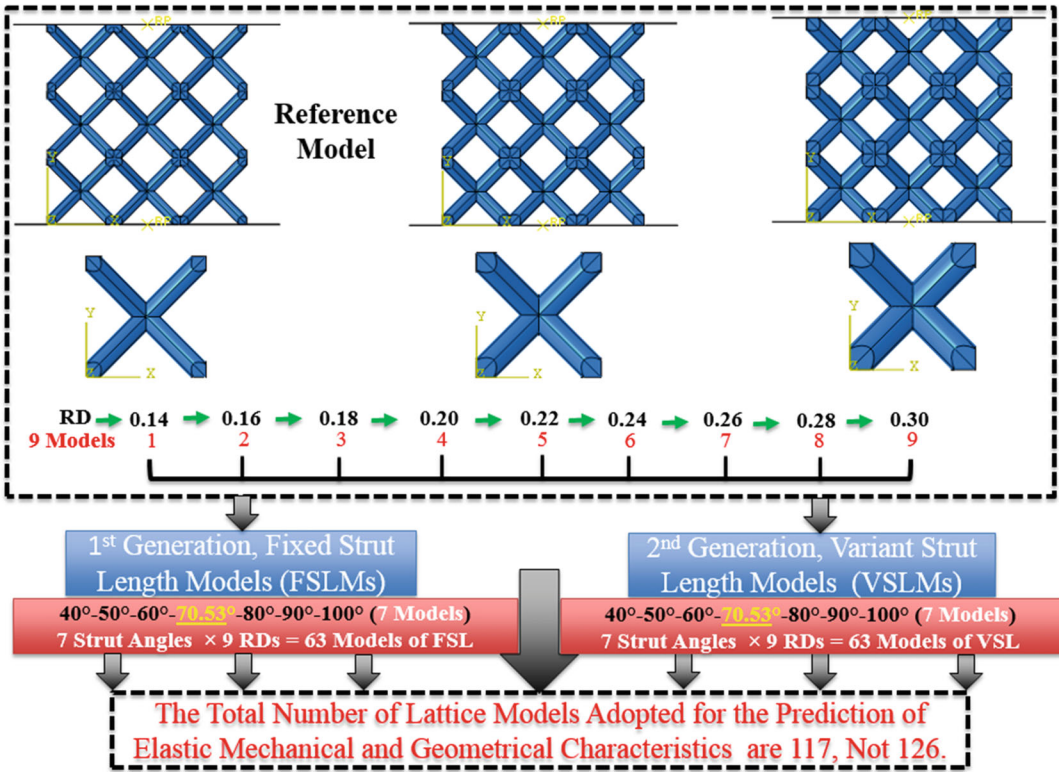

FIGURE 3 Classifications of the modified BCC LSs adopted in the current research with respect to the strut angles, strut length and RDs

applied to each modified BCC LS in both FSLMs and VSLMs, starting with an initial value for the strut radius and then building the entire lattice model with ABAQUS FE software. After that, the actual lattice volume and the overall lattice block volume of the generated model were measured by using ABAQUS diagnostic tool to determine the RD. Then, the resultant value will be compared with the required or target one in order to check whether the assumption or the initial value of the strut radius is correct or not. If the resultant one matches with the required RD, it means that the initial value of the strut radius is correct. While in the case that the value of the resultant RD and the target one does not agree with each other, another assumption will be initiated based on the feedback from the difference between these two values. The last procedure will be repeated several times till estimating the exact strut radius and the associated geometries corresponding to each RD within the specified range for all lattice models in both sets. In consequence, 63 lattice models of fixed strut length listed within the FSLMs and other 63 models of variant strut length considered as a part of the VSLMs have been generated. Thus, as shown in Figure 3, the total number of models adopted in the current research is 117 models, not 126, owning to the repetition of 9 RMs corresponding to 70.53° strut angle with 9 different RDs of the specified range. To this end, since the parametric study can take a longer time for generating the lattice models of various RDs, empirical closed-form equations relating the RD with strut radius will be created based on the data of the geometries for the 117 models. This in turn aims to determine strut radius directly without the need for applying further parametric studies. Also, these equations will be provided in the result and discussion part, Section 5.3.2.

4 | FINITE ELEMENT MODELING

All the models adopted in the current investigation were built and analyzed explicitly using ABAQUS/CAE 2016 from Dassault Systemes, Providence, RI, USA. Elastic–plastic FE simulation (including strain hardening) of a quasi-static axial compression test was conducted on all modified BCC LSs by defining the material properties and boundary conditions, estimating elastic modulus and yield stress, generating the appropriate mesh type, applying mesh convergence analysis, and studying the effect of lattice cell tessellations.

4.1 | Material properties

The solid constitutive material assigned to all elastic–plastic FE models was acrylonitrile butadiene styrene (ABSplus-P430). This material was adopted here since it is widely used in the field of additive manufacturing or 3D printing technology. In this regard, Table 1 shows ABS properties, where this data were already measured and introduced in the literature by conducting standard tensile (ASTM D882) and compression (ASTM D695, ISO 604) tests on ABS specimens fabricated by FDM technology.[29,30,35,36] Up to this point, the mechanical behavior of solid ABS material, that is, the printed one based on a layer-by-layer fabrication approach using fused deposition modeling technology, was assumed to be isotropic for the purpose of modeling simplification.

4.2 | Boundary conditions

In order to simulate the quasi-static axial compression behavior of the lattice, each model of the modified BCC LSs was placed between two rigid plates, as shown in Figure 4, which are tied to the upper and lower faces of the lattice. The boundary conditions were assumed based on the experimental observation. For the base plate, fixed boundary conditions were used, which are ENCASTER (U1 = U2 = U3 = UR1 = UR2 = UR3 = 0). Whereas for the top plate, moveable boundary conditions were conducted by applying a displacement in Z directions (U3), and all other directions were restricted and kept zeros (U1 = U2 = UR1 = UR2 = UR3 = 0).[37,38] In this regard, the other four faces or sides of the lattice are totally free or unconstrained. In general, LS under these types of conditions is referred to as a constrained lattice.[26] Additionally, the displacement rate was 0.5 mm/min, which is identical to the displacement rate used for the experimental work.[30,35] The solver used to run the models of the current study is Abaqus/Explicit, aiming to create general-purpose models that could be used in the future to predict post-yielding behavior.[13] To this end, two steps (Initial STEP and STEP1) were used, and the computational time required for a single analysis is usually within the range from 10 to 20 min based on lattice geometries.

TABLE 1 ABS properties

Quantity	Observation	Value
ABS Poison's ratio	ν	0.35
ABS density	ρ	7.92E-4 g/mm^3
Yield stress	σ_Y	861.5 MPa
Ultimate failure strength	σ_u	33.32 MPa

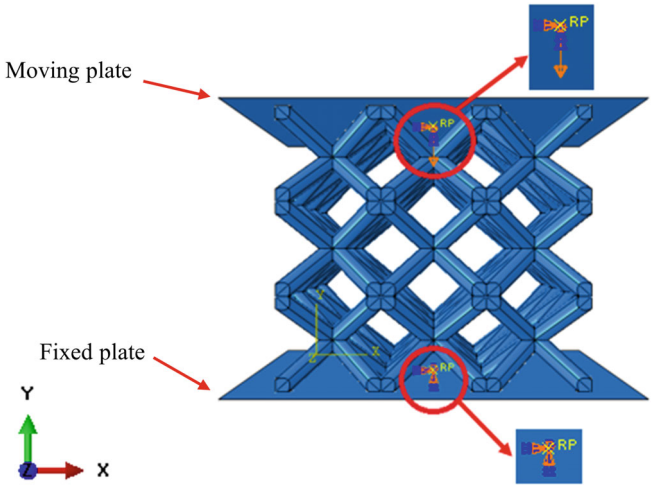

FIGURE 4 The applied loading and boundary conditions of the finite element modeling

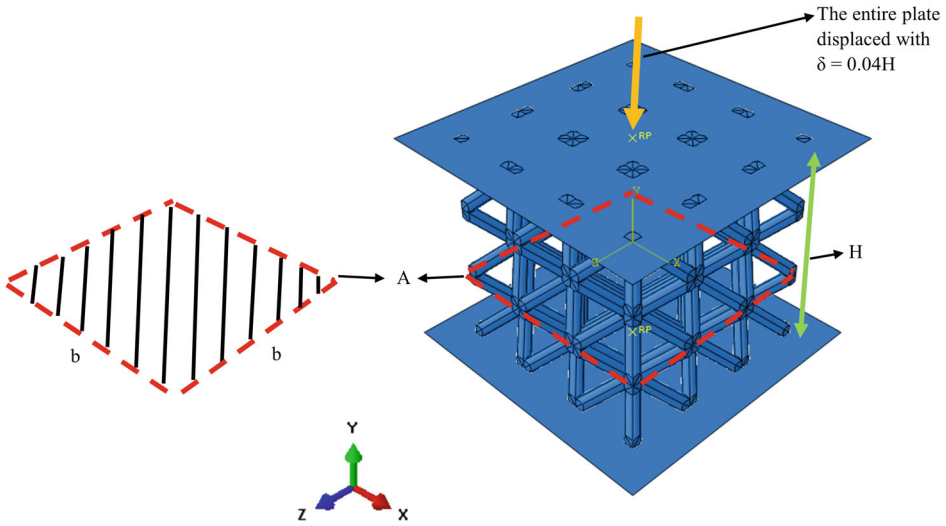

FIGURE 5 The essential geometries required for determining the elastic modulus of the lattice

4.3 | Elastic modulus and yield stress estimation

In order to estimate the elastic modulus of the modified BCC LSs in the direction of applying the displacement, the reaction force was measured at the upper plate and the associated data were extracted from ABAQUS and exported to an Excel file in order to plot the load–displacement curve.

The slope of the curve represents the load–displacement stiffness, denoted by K measured in (N/mm). Hence, the elastic modulus was determined as follows.[16,17,23,39,40]

$$E = \frac{\sigma}{\varepsilon} = \frac{\frac{F}{A}}{\frac{\delta}{H}} = \frac{H}{A} \times \frac{F}{\delta} = \frac{H}{A} \times K, \tag{1}$$

where E is the modulus of elasticity, sometimes called equivalent elastic modulus since it represents the modulus of the whole LS, as well as to distinguish it from the one of solid constitutive material, measured in (MPa). Also, δ is the applied compressive displacement, H is the total height of the lattice and A is the cross-sectional area of the lattice. All of these are explained as shown in Figure 5 and measured in (mm), (mm), and (mm^2), respectively. Regarding the yield stress of the lattice, it is also called the crush or collapse stress. Indeed, it comes directly after the end of the elastic region where the curvature of the load–displacement plot starts, or it represents the beginning of the plateau regime where the collapse or crush of the cell struts begins. At this point, a new deformation mechanism of the cell struts could be noticed.[41] To this end, it is important to indicate that the lattice yield stress signifies the equivalent yield stress of the entire LS and does not stand for the real stresses in individual struts.[14]

4.4 | Mesh generation

The most widely used elements in finite element analysis (FEA) are tetrahedron and hexahedron. The former can be generated automatically, while the latter requires an intervention by the software users.[42] The hexahedral elements are generally more preferred than tetrahedral elements. Because employing hexahedral mesh elements in FEA leads to reducing the computational time and increasing the accuracy of the results.[43] Accordingly, all the models in the current research have been meshed with hexahedral elements using smart procedure. It is a meshing technique developed in ABAQUS software for the purpose of generating hexahedral elements. This procedure was presented in our earlier study,[44] and proved to work efficiently in generating hexahedral elements for all modified BCC LSs (i.e., FSLMs and VSLMs).

In short, to create a mesh for a certain model that cannot be meshed directly with hexahedron elements, a volume decomposition is required for its geometries. It means that certain planes should be allocated at the right positions to

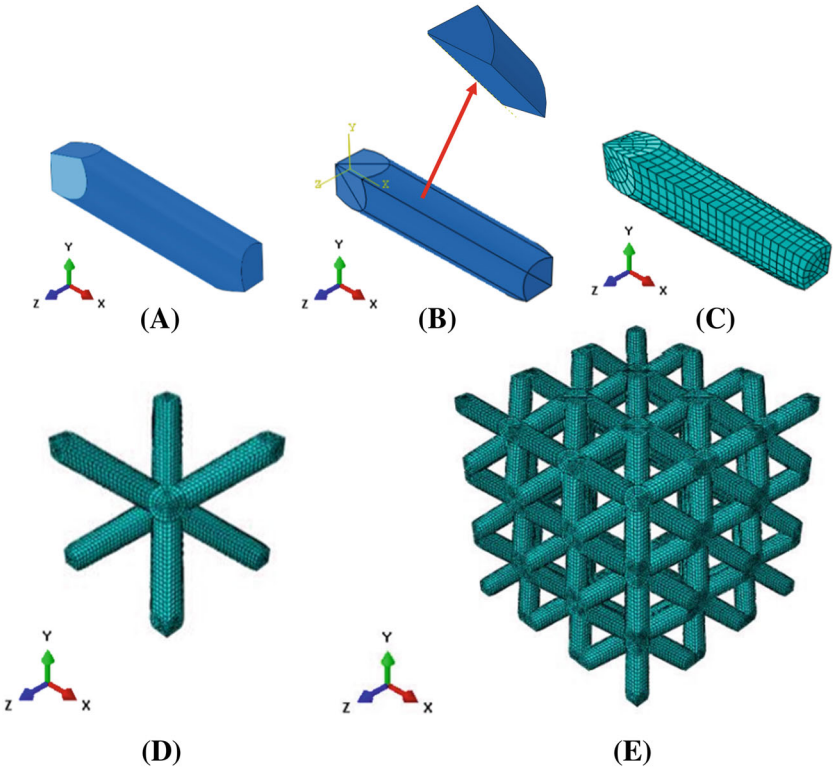

FIGURE 6 Creating (A) solid single strut, (B) single strut with volume decomposition, (C) meshable single strut, (D) meshable unit cell, and (E) entire lattice meshed with hexahedron elements

partition the entire model or part into subparts. These subparts are similar to the ones provided by ABAQUS library that could be self-meshed with hexahedron elements; by this way, the entire model could be meshed with hexahedron elements directly. The same idea was applied as a part of smart procedure on the lattice models. Starting with a single strut as shown in Figure 6A, three planes are used to split the strut geometry into six subparts as shown in Figure 6B. The subparts of the single strut have the same geometrical features as those of ABAQUS library that could be meshed directly using hexahedron elements. Then, the hexahedron mesh is generated automatically for the single strut as seen in Figure 6C. This type of mesh is maintained even with creating a single unit cell and entire lattice structure as shown in Figures 6D,E, respectively.

Also, the element type was selected to be continuum stress-displacement, 3D (three-dimensional, break, or solid element), first order interpolation (i.e., linear behavior), and reduced-integration (i.e., one sampling point to determine numerically the stiffness and mass of the element). This element is designated as C3D8R according to ABAQUS scheme. For more explanation, the first order reduced-integration elements are cheaper and more effective than first-order full-integration elements due to their capability for removing shear locking, overcoming hour glassing with using several elements in the thickness direction, and saving computational time. However, the elements with Incompatible mode C3D8I were tested for this study, and it was observed to exhibit higher computational time. Finally, the relative elastic modulus of the entire lattice was selected to apply a convergence analysis. The seed size or number of elements was varied several times, and the corresponding relative elastic modulus was determined. This process continued till reaching a convergence in the values of the relative elastic modulus with insignificant error, which is less than 2% when the number of elements became 220,000 or higher as will be discussed in Section 4.5 (mesh convergence analysis and the effect of unit cell number). By this way, we could guarantee that the finite element models will provide accurate results. For the top and bottom plates, a planar element type (R3D4) with a discrete rigid characteristic was chosen because of its higher elastic modulus such that it will not undergo deformation under any type of loading conditions. In this regard, the upper and lower rigid plates were fixed on the corresponding lattice faces. This means constrained boundary conditions between the lattice and plates were used. In consequence, the rigid plates and the constrained boundary conditions as well as employing hexahedron mesh elements for both lattice and plates ensured a good compatibility, especially that high deformation stages were not included in this research.

4.5 | Mesh convergence analysis and the effect of unit cell number

It has been found that mechanical characteristics of lattice are influenced by the number of unit cells due to the effect of boundaries.[16,17,45] To explain that, a preliminary study for the effect of unit cell number on the elastic–plastic mechanical behavior of lattice (engineering stress–strain curve) was carried out by using FE modeling of the quasi-static axial compression test considering the same boundary conditions, mesh element type and the other details discussed earlier. Corresponding to each unit cell number as an essential step, the mesh convergence analysis was conducted between the RE and the number of elements per unit cell to ensure that the results are accurate enough. In this regard, the number of elements per unit cell is considered a kind of normalization, which means that the total number of elements for a certain model is divided by the number of unit cells out of which it is built.[17,46] It has been noticed that the convergence error can be reduced to insignificant values by using the number of elements per unit cell higher than or equal to 2000 for all lattice cell repetitions. Simply, multiplying that number, 2000, with the number of unit cells ranging from $1\times1\times1$ to $5\times5\times5$ yields the corresponding total number of elements with a range from 2000 to 250,000. In consequence, the effect of lattice cell tessellations on the elastic–plastic compressive mechanical behavior using the above results of convergence analysis is shown in Figure 7, for the RM of 0.3 RD or 0.6747 mm strut diameter.

As noticed in Figure 7, the mechanical response is relatively high for $1\times1\times1$ lattice cell tessellation due to the constrained boundary conditions and the direct effect of the boundary conditions, which are applied on all solid struts of a single unit cell. However, that effect is reduced with increasing the number of unit cells since the cells located at the boundaries are decreased in number with respect to the total number of unit cells out of which the LS is composed. This means that smaller number of cell struts with respect to the total number of struts are under the impact of boundaries. Thus, the mechanical behavior and the corresponding CMPs clearly begin approaching each other for $3\times3\times3$, $4\times4\times4$, and $5\times5\times5$ unit cell distributions. For this reason, the last three lattice cell arrangements were frequently used in the literature by several researchers.[16,17,47,48] In the current research, $3\times3\times3$ lattice cell tessellation was selected to simulate the elastic–plastic compressive mechanical behavior of all modified BCC LSs in both sets for the purpose of saving further computational time. In other words, all the results regarding the strut angle variation and changing the RD with considering both the fixed and variant strut length as design constraints will be provided for $3\times3\times3$ unit cell repetitions in the next sections. Using the former lattice cell tessellation, a convergence analysis was conducted on the seven models of fixed strut length and the other seven models of variant strut length with 30% RD and strut angle variation from 40° to 100° as shown in Figures 8 and 9, respectively. As a result, the total number of elements that reduce the convergence error to insignificant values is higher than or equal to 50,000, corresponding to all lattice models of fixed and variant strut length with 30% RD. In a similar way, as a convergence study was conducted on other lattice models of different RDs, it was significantly observed that the same number of elements can also provide reasonable results.

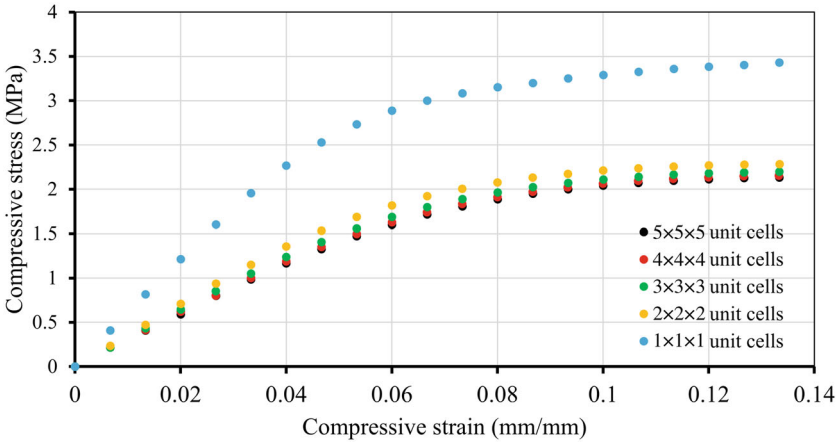

FIGURE 7 The effect of cell repetitions on the elastic–plastic mechanical response of the lattice, starting with $1\times1\times1$ to $5\times5\times5$ unit cells for the RM of 0.3 RD.

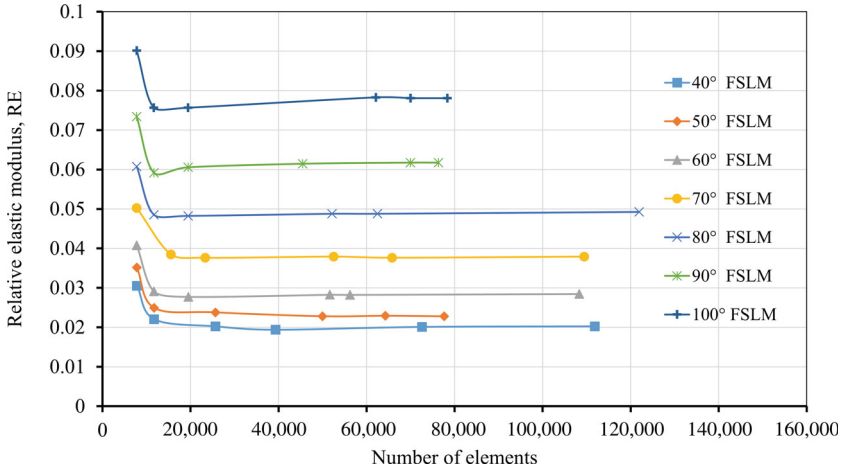

FIGURE 8 Mesh convergence analysis of the seven models in the FSLMs of 0.3 RD and strut angle variation from 40° to 100°

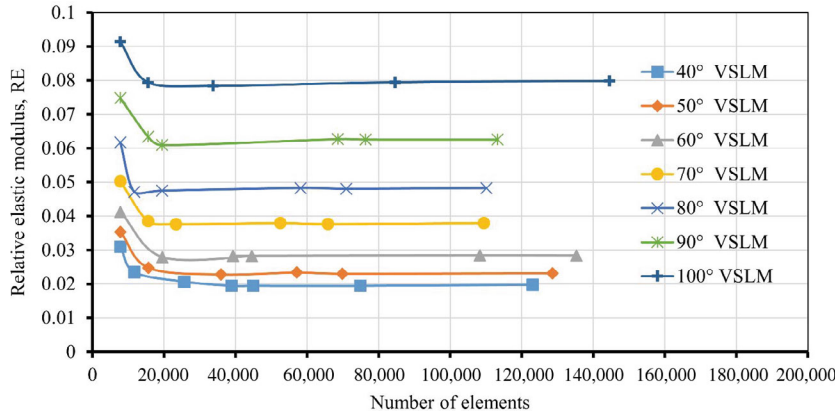

FIGURE 9 Mesh convergence analysis of the seven models in the VSLMs of 0.3 RD and strut angle variation from 40° to 100°

5 | RESULTS AND DISCUSSION

5.1 | Comparison between experimental work and FE models

Load–displacement curves obtained experimentally by compression test were compared with the corresponding one of the FE simulations for the reference model as shown in Figure 10. It is obvious that the mechanical response for both the experiment and FE model was within the linear elastic limit since the applied displacement is relatively small. Significantly, a good agreement was noticed between the load–displacement curve predicted by the FE model and those of experimental work. The average value and standard deviation of the measured load–displacement stiffness by experiment were 149 and 2.8% in N/mm unit, respectively. Comparing with the load–displacement stiffness of FEM (154.19 N/mm), there is a discrepancy in the results with a small percentage (i.e., 3.37%). The sources of discrepancy are various; for example, human error is a very common source of error when conducting an experimental work. Also, the defects shown in the printed samples due to the manufacturing parameters might be another source of discrepancy. In general, this amount of discrepancy is considered small, and it could be neglected since it has not major effect on the results. Up to this point, the boundary and loading conditions were validated for the reference model. Hence, the same conditions were adopted for all other models in this study to make sure these models could work efficiently and provide accurate results.

5.2 | Mechanical characteristics of the modified BCC LSs

After the elastic–plastic FE simulation of the quasi-static axial compression behavior of all modified BCC LSs, elastic modulus and yield stress corresponding to each lattice model were determined using the same ways explained in Section 4.3.

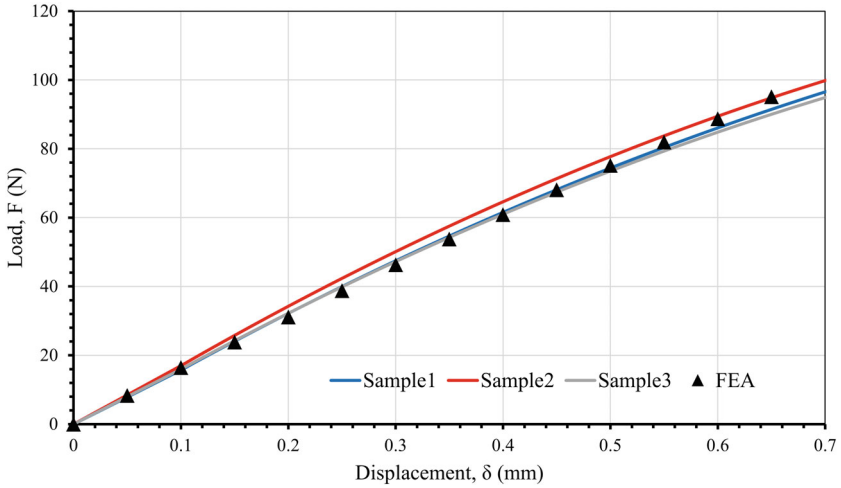

FIGURE 10 The load–displacement behavior within elastic limit of the RM under compressive loading for both the FE model and experimental work

To provide the readers with better understanding, the quasi-static compression behavior means that the piston or platen used to apply compressive loading on the lattice samples moves very slowly, thereby inducing a very slow deformation such that the inertial effects could be ignored. Also, the influence of the acceleration on the instrument measuring compressive loading is insignificant and could be neglected too.

5.2.1 | Elastic modulus and yield stress of FSLMs and VSLMs

The measured data of elastic modulus and yield stress corresponding to the strut angle variation and RD values of all lattice models were normalized relative to the modulus and yield stress of the solid constitutive material, respectively. These data were thereafter fitted with Gibson and Ashby's scaling laws, illustrated in Equations (2) and (3).

$$RE = c_1(RD)^n, \tag{2}$$

$$RS = c_5(RD)^m, \tag{3}$$

$$RE = \frac{E_{latt.}}{E_{sol.}},$$

$$RS = \frac{Y_{latt.}}{Y_{sol.}},$$

$$RD = \frac{V_{latt.}}{V_{sol.}},$$

where $E_{latt.}$, $Y_{latt.}$, and $V_{latt.}$ are the equivalent elastic modulus, the effective yield stress, and the actual volume of the lattice, measured in MPa, MPa, and mm^3 units, respectively. In addition, $E_{sol.}$ and $Y_{sol.}$ represent the modulus of elasticity and the yield stress of the solid constitutive material that the lattice is made of, both measured in MPa units. In addition, $V_{sol.}$ refers to the overall lattice block volume, measured in mm^3 units. c_1, c_5, n, and m are indicated as Gibson and Ashby coefficients.

After data fitting with the scaling laws, the coefficients (c_1 and n) were determined for both FSLMs and VSLMs as shown in Figures 11 and 12, respectively, thereby providing empirical closed-form equations through which the elastic modulus of the modified BCC LSs can be controlled by varying the RDs for different strut angles and two design sets (FSLMS and VSLMS). In this respect, all the values of c_1 are within the range specified by Gibson and Ashby, that is, 0.1–4.[10,11] Besides, the values of n are of high importance not only for predicting elastic modulus values but also for analyzing how the deformation mechanisms of LSs can change with strut angle variation, which has a major influence on the

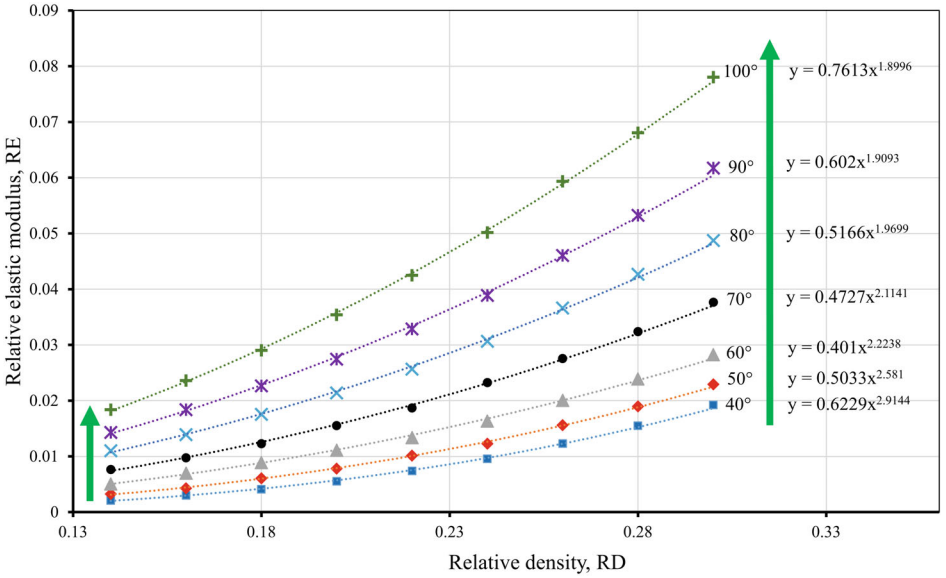

FIGURE 11 Empirical closed-form equations relating RE with RD for FSLMs ensued from fitting ABAQUS data with the scaling laws

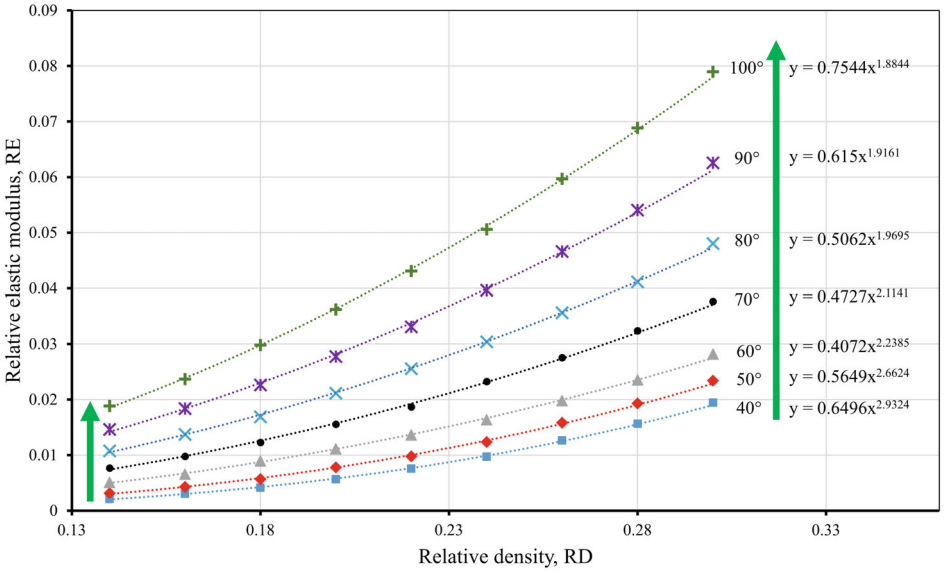

FIGURE 12 Empirical closed-form equations relating RE with RD for VSLMs ensued from fitting ABAQUS data with the scaling laws

associated mechanical characteristics. Accordingly, the n-values were plotted separately with strut angles for both FSLMs and VSLMs as shown in Figures 13A,B, respectively. Based on the latter, it can be seen apparently that the exponent values of both sets are approximately similar to each other and decreases with increasing the strut angles, giving a conclusion that the main deformation moves toward axial loading rather than bending of the struts with increasing the strut angles. For this reason, RE values go up with increasing the strut angles for a given value of the RD. Furthermore, it has been frequently reported in the literature that the RE of a lattice increases with increasing the RD values.[10,12,17,18,20,21,25,49–51]

Similarly, in the current work, the values of RE also increase with increasing the RD for both FSLMs and VSLMs as shown in Figures 11 and 12, corresponding to a certain strut angle. In addition, it was noticed that values of c_1 and n of the RM are approximately similar to the ones arising from the previous investigations,[14,52] which were also conducted on BCC LSs. Most importantly, it was observed from Figures 11 and 12 that c_1 and n have roughly the same values for both FSLMs and VSLMs when making a comparison between two lattice models of similar strut angles and RDs but from different sets, thereby revealing the dominant effect of the strut angles on the elastic modulus values. Up to this end, a validation of

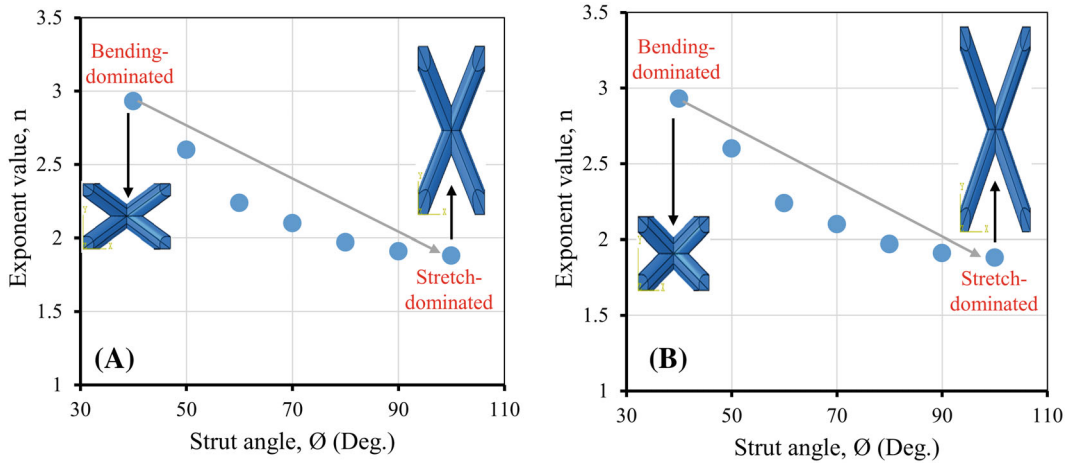

FIGURE 13 The trend of exponent values (n) with strut angle variation for (A) FSLMs and (B) VSLMs

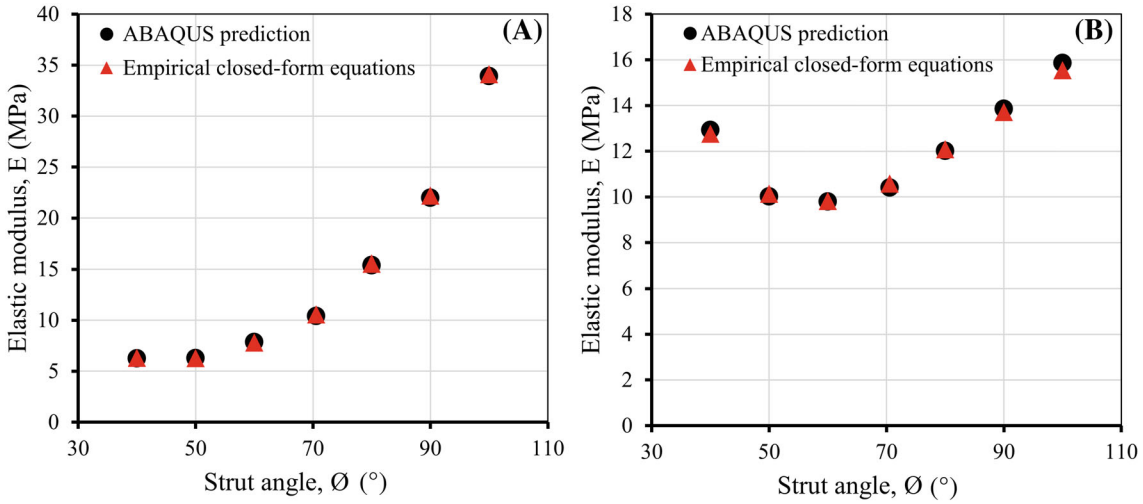

FIGURE 14 Validation of the empirical closed-form equations relating RE with RD for (A) FSLMs and (B) VSLMs with respect to ABAQUS prediction from the previous work

the empirical closed-form equations was carried out by testing their abilities for predicting the elastic modulus behavior with strut angle variation of the constant and variable weight models which were presented in the previous study.[44] The modified BCC LSs of constant and variable weight were simulated based on ABAQUS FE software using acrylonitrile butadiene styrene (ABS) material. As it can be seen from Figure 14A,B, there is a good agreement between the results of the empirical equations and ABAQUS FE software.

In a similar way, the constants (c_5 and m) were found as shown in Figures 15 and 16, resulting in another set of empirical closed-form equations to predict directly the yield stress by changing the RD for all modified BCC lattice models in both sets. Again, the constants of FSLMs were noticed to be approximately similar to the corresponding ones of VSLMs. The values of the scaling factor (c_5) were found to be almost within or close to the range specified by Gibson and Ashby, which is between 0.1 and 1.[11] Furthermore, the coefficients (c_5 and m) of the RM were found to be nearly the same as those from an earlier investigation conducted by Reference 52 on BCC lattice configuration. Similar to the elastic modulus trends, the yield stress increases with increasing RD at a given strut angle, and it goes up with increasing the strut angle at a specific value of RD. This means the general tendency for changing the deformation mechanisms from bending- to stretch-dominated with maintaining the same RD induces an improvement not only in the elastic modulus but also in the yield stress for all modified BCC LSs.[12,48,52–54] Indeed, changing the deformation mechanisms for the purpose of improving the mechanical response of the lattice was conducted before, conventionally by adding vertical struts in the

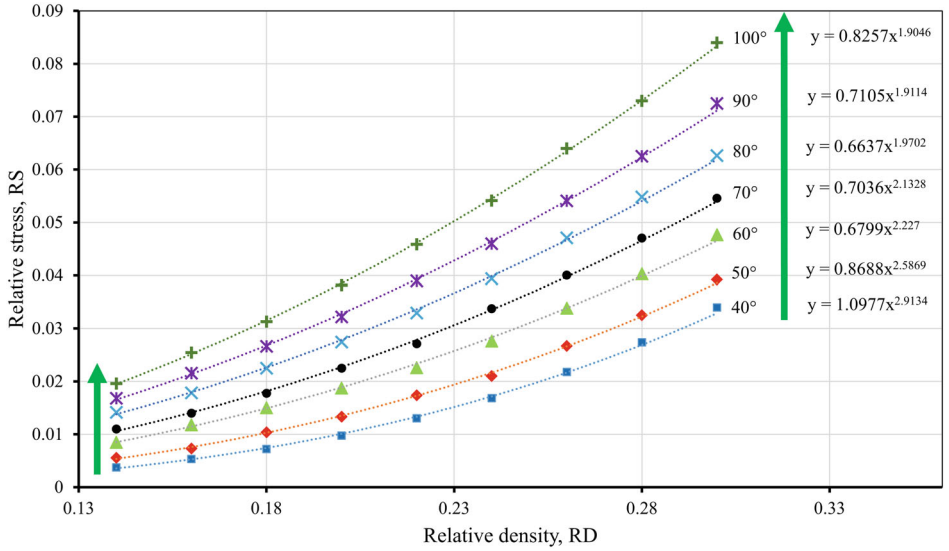

FIGURE 15 Empirical closed-form equations relating RS with RD for FSLMs ensued from fitting ABAQUS data with the scaling laws

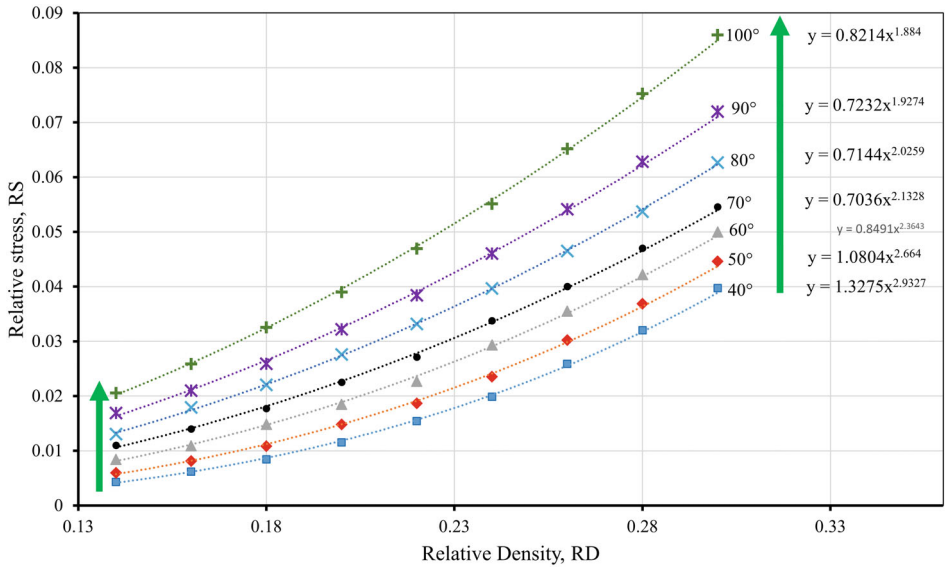

FIGURE 16 Empirical closed-form equations relating RS with RD for VSLMs ensued from fitting ABAQUS data with the scaling laws

direction of applying the load to the basic feature of BCC LS to create other features, thereby exhibiting higher CMPs at the same RD.[4,14,21,51–53]

In the current research, the leverage of switching the deformation mechanisms toward axial mode instead of bending the struts was used by reshaping the actual lattice volume or weight of BCC LS longitudinally in the load direction to create other features of different strut angles starting from 40° to 100°, thereby offering higher values of elastic modulus and yield stress at the same RD. The improvement in the CMPs is attributed to the ability of the lattice to resist more axial deformation under compressive loading when changing strut angles in the direction of applying the load, which means improving the structural stability of the lattice by increasing the strut angles. Eventually, in a similar fashion to the validation of elastic-modulus empirical equations, it is worthwhile indicating that there is a good agreement between the yield stresses predicted directly by the empirical closed-form equations and those extracted from ABAQUS FE models as shown in Figure 17.

It has been observed that some values of the coefficients (c_1, c_5, m, and n) resulting from the current investigation might be close to the upper limit, lower limit, or even beyond the range of values specified by Gibson and Ashby,

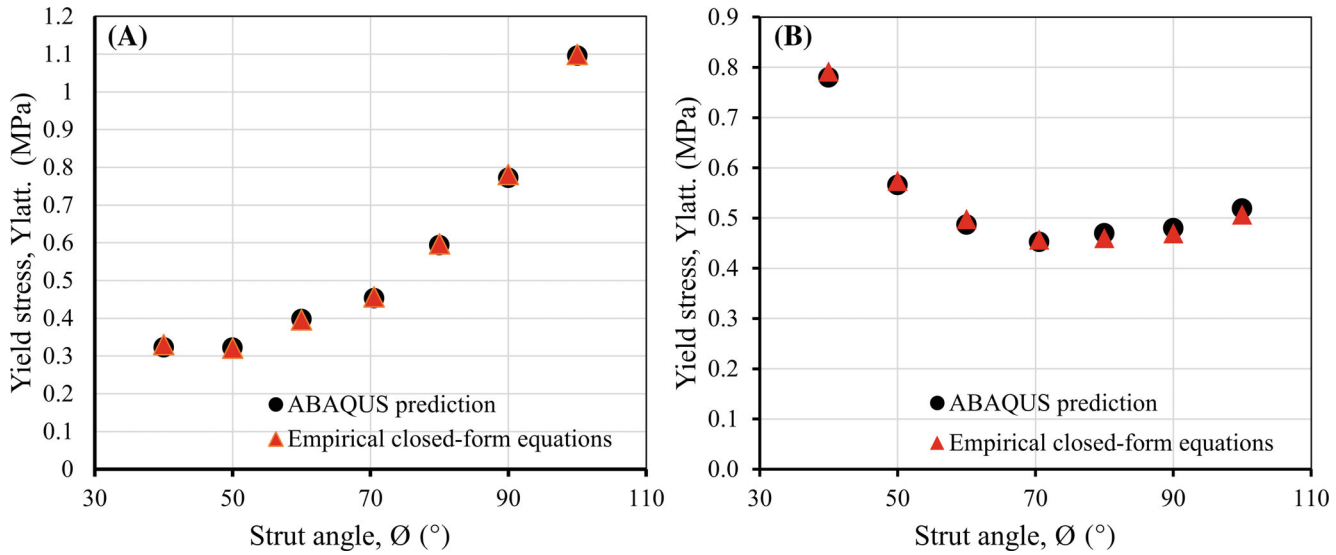

FIGURE 17 Validation of the empirical closed-form equations relating RS with RD for (A) FSLMs and (B) VSLMs with respect to ABAQUS prediction from the previous work[44]

c_1=(0.1–4), c_4=(0.1–1), m = (2 or 1), and n = (1.5 or 1).[10–12,19] This can be traced back to the fact that the geometrical shape of lattice unit cells and their distribution in the 3D-space, that is, whether distributed in a periodic or stochastic way, have an influence on these coefficients,[14,50,55] especially that Gibson and Ashby's model is an open-foam stochastic cellular structure, while all the lattice models adopted in the current research were modified BCC LSs with regular distribution of the unit cells. In this regard, it has been shown in the literature that the polymeric BCC and reinforced-BCC lattice configurations have different values of c_1 and c_5 even though they were manufactured with the same RD, thereby showing the dependency of these coefficients on the type of lattice unit cell.[14] Besides, it has been reported that the scaling factor (c_5) of titanium triply periodic minimal surface (Ti-4 V-6Al TPMS) LSs was found to be out of the range specified by Gibson and Ashby with the values (1.31 and 1.39) for gyroid and diamond, respectively, which is in turn attributed to the same reasons mentioned above regarding the shape and distribution of the lattice unit cells, as well as the residual stresses and the irregularities in the struts due to manufacturing process.[50] Also, it has been observed based on FEMs that the exponent (n) can have a range of values within (0.8–2.6) for polymeric TPMS and BCC LSs.[17] In related work, it was characterized the state of deformation for photopolymer-resin TPMS LSs (P- and G-type) as a stretch- and bending-dominated with n-values, 1.741 and 2.256, respectively.[47] Likewise, it has also been found that the exponents (n) and (m) can have a range of values (between 0.92 and 2.84), and (between 1.75 and 3.5), respectively, for different periodic metal LSs.[4,18] In short, this means that n-values are not necessary to be 2 and 1 for bending- and stretch-dominated structures, respectively. In essence, these coefficients are dependent on the topology of the unit cells and the direction of applying the load, as well as the other factors associated with the manufacturing process.[14,17,47,50]

5.3 | Structural parameters of the modified BCC LSs

Not only predicting the CMPs of modified BCC LSs is of such importance in the field of lattice design but also predicting the associated structural parameters is of similar interest. Since any LS should have a unique combination of relatively high strength and lightweight in its intrinsic feature in order to make the required design feasible and functional. Regarding this combination, the former is related to the mechanical performance of the lattice while the latter is associated with the structural parameters. For this reason, in the current section, empirical closed-form equations will be created to predict the actual lattice volume, strut diameter, aspect ratio, and the overall lattice block volume, all with respect to the RD for the modified BCC LSs in both sets.

5.3.1 | Actual lattice volume of FSLMs and VSLMs

The actual lattice volumes of all models in both sets were measured precisely using ABAQUS diagnostic tool with considering the material distribution at strut joints. Then, they were correlated with the RD to generate the corresponding

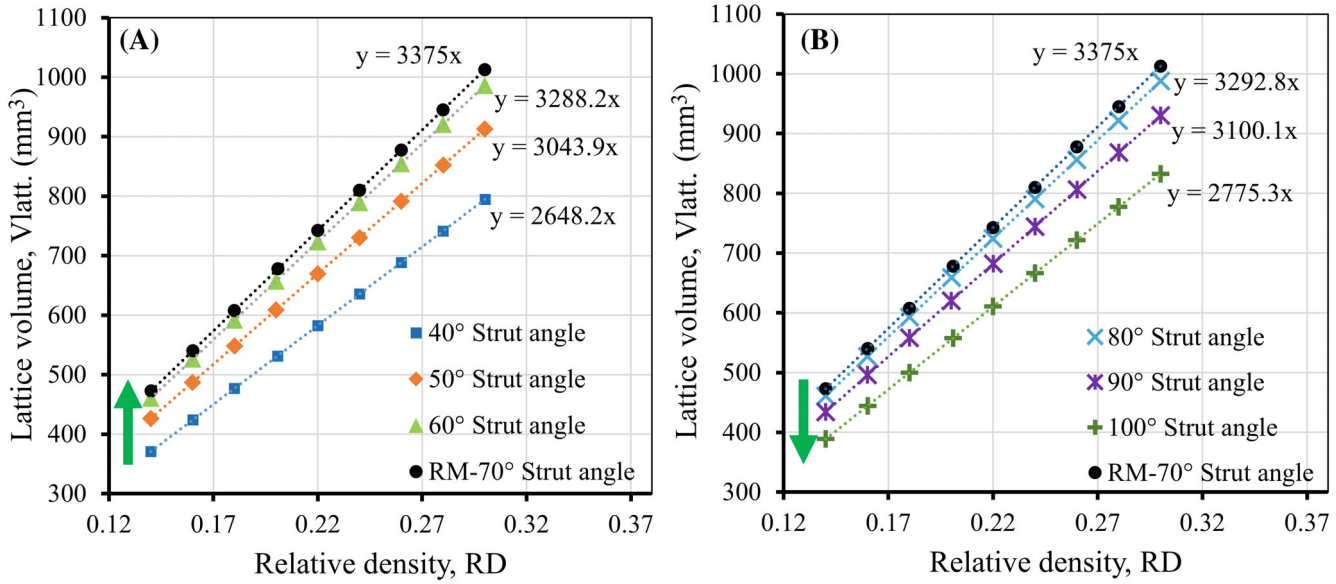

FIGURE 18 Empirical closed-form equations correlating actual lattice volume with RD of FSLMs for strut angles (A) less and (B) higher than 70°

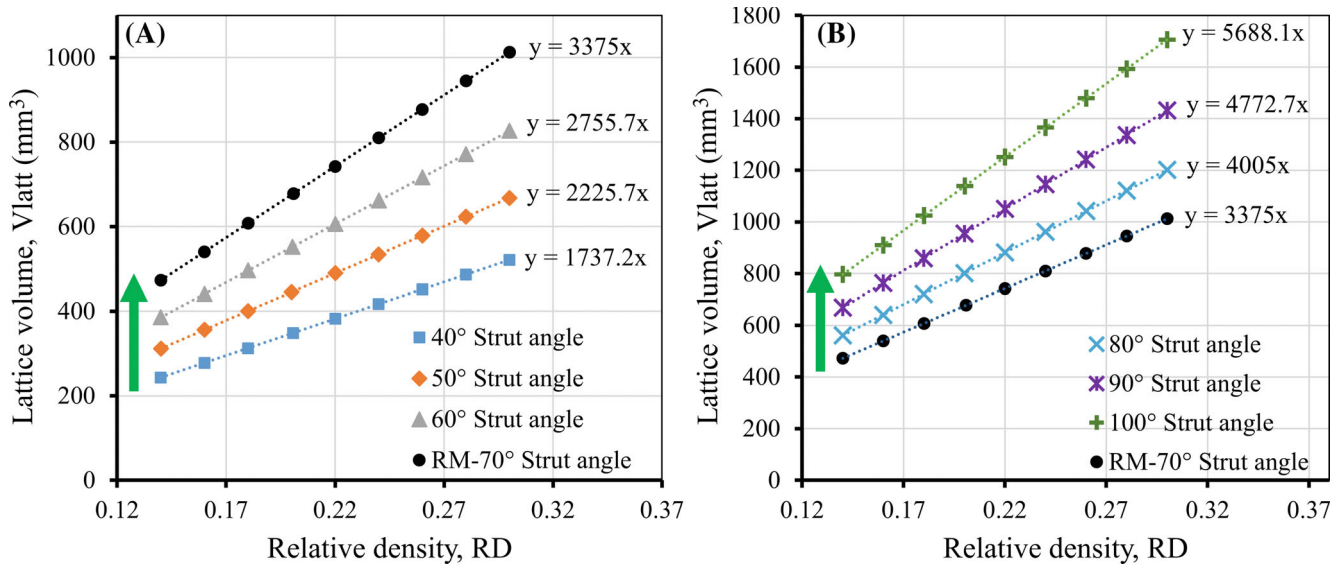

FIGURE 19 Empirical closed-form equations correlating actual lattice volume with RD of VSLMs for strut angles (A) less and (B) higher than 70°

empirical closed-form equations for both FSLMs and VSLMs as shown in Figures 18 and 19. Obviously, there is a linear relationship between the actual lattice volume and RD for all models in both sets.

Also, it has been found that the actual lattice volumes of FSLMs increase with increasing the strut angles, only for strut angles lower than 70° as shown in Figure 18A, and decrease with increasing the strut angles for strut angles higher than 70° as shown in Figure 18B. Whereas, the actual lattice volumes of the VSLMs increase monotonically with increasing the struts angles for both strut angles lower and higher than 70° as shown in Figure 19A,B, respectively. This is due to the fact that the strut length of VSLMs is not fixed. Indeed, it goes up with increasing the strut angles. In addition, it is worth noting that the VSLMs of strut angles (40°, 50°, and 60°) offer actual lattice volumes lower than their counterparts of FSLMs since the strut lengths of the VSLMs corresponding to strut angles (40°, 50°, and 60°) are lower than the corresponding ones of FSLMs which have a fixed strut length equal to the one of the RM. However, the reverse occurs with the VSLMs of strut

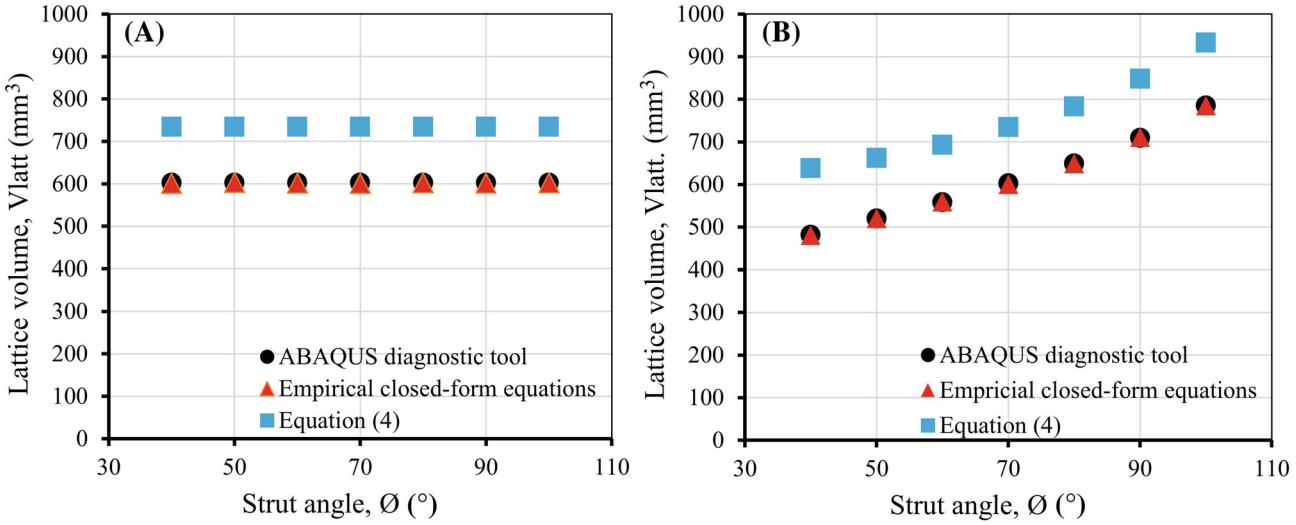

FIGURE 20 Validating the results of the empirical closed-form equations relating actual lattice volume with RD for (A) FSLMs and (B) VSLMs with respect to those of ABAQUS diagnostic tool from the previous study and comparing them with those of Equation (4)

angles (80°, 90°, and 100°). That means, since they have strut lengths higher than corresponding ones of the FSLMs, their actual lattice volumes are expected to be higher than those of FSLMs. Furthermore, it has been demonstrated that these equations work well in predicting accurately the actual lattice volumes of all lattice models in both sets by comparing their results with the corresponding ones of the ABAQUS diagnostic tool from the previous study,[44] that is, the constant and variable weight models as shown in Figure 20. The good agreements between the results are attributed to considering the influence of material distribution at strut junctions when creating the current empirical-closed form equations, thereby making them more efficient and practical than the geometrical Equation (4), listed below. The latter is the same as other geometrical equations, which were invoked in the literature by several researchers.[26,27,56,57]

$$V_{latt.} = 4\pi R^2 \times \sqrt{X^2 + Y^2 + Y^2} \times N^3, \tag{4}$$

where R is the strut radius and N is the number of unit cells in a certain direction assuming that the entire LS has the same number of unit cells in all directions. Besides, X, Y, and Z represent the unit cell edges or dimensions in the x, y, and z directions, respectively. Significantly, the actual lattice volume determined by the above-mentioned equation was not accurate enough comparing with the results of both the ABAQUS diagnostic tool and the empirical closed-form equations developed in the current study as shown in Figure 20. This is due to not taking into account the material overlapping at strut joints, resulting in a discrepancy in the results. Accordingly, the aforementioned equation or the other geometrical equations introduced in the literature were limited to small RDs. In this regard, the values of the actual lattice volume estimated by Equation (4) were higher than those of the ABAQUS diagnostic tool and the empirical closed-form equations as can be noticed in Figure 20. The reason for that was attributed to overestimating the actual lattice volume at strut junctions by four times, which in turn has a major impact on the corresponding values of RD and the associated values of the RE and RS.

5.3.2 | Strut radius of FSLMs and VSLMs

The data of strut radius were determined corresponding to all modified BCC LSs based on the parametric study conducted in Section 3 by using ABAQUS diagnostic tool. Afterward, they were correlated with the values of RD to generate empirical-closed form equations corresponding to each strut angle of the FSLMs and VSLMs as shown in Figures 21 and 22, respectively. Based on that, there is a power-function relationship between the strut radii and RDs with an exponent value around 0.57 for all lattice models of different strut angles in both sets. In general, the trends of strut radius with RD are similar to those of actual lattice volumes with RDs for both FSLMs and VSLMs. In addition, there is no need

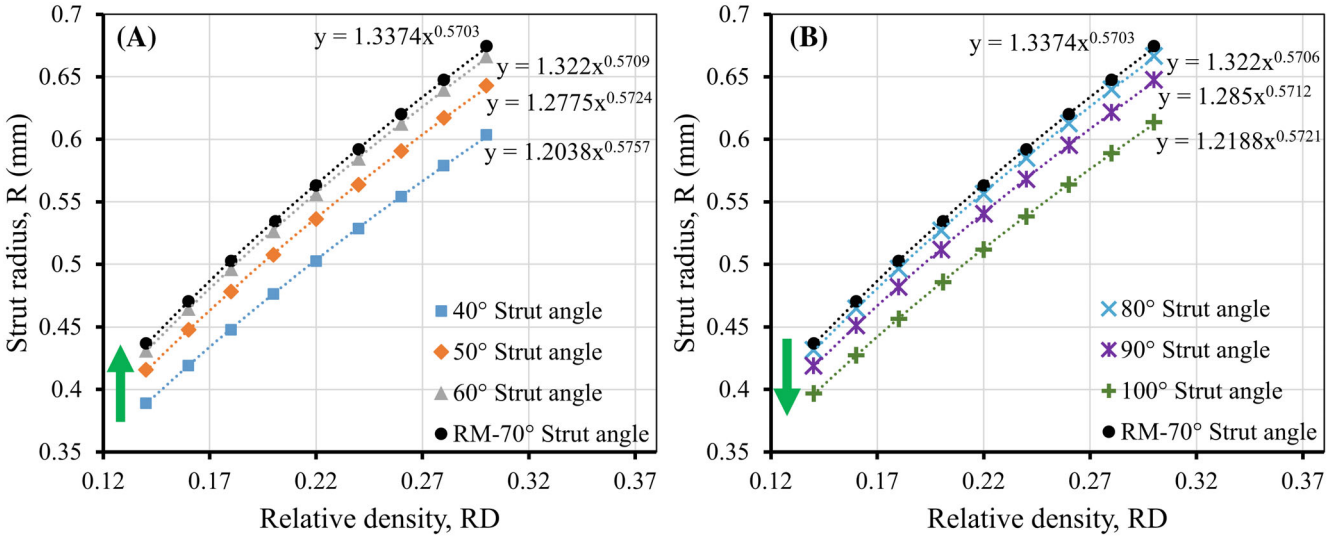

FIGURE 21 Empirical closed-form equations correlating strut radius with RD of FSLMs for strut angles (A) less and (B) higher than 70°

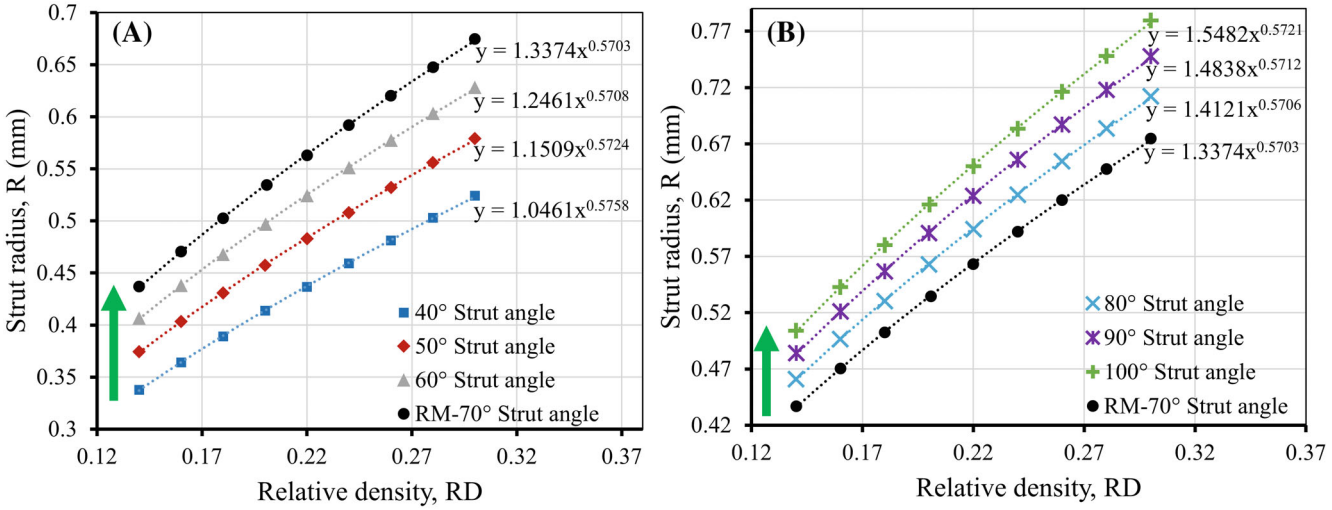

FIGURE 22 Empirical closed-form equations correlating strut radius with RD of VSLMs for strut angles (A) less and (B) higher than 70°

to validate the closed-form equations of the strut radius since all the geometries are related together. This means that if the empirical closed-form equations required to estimate the actual lattice volumes with respect to RDs provide accurate results, the corresponding ones of the strut radius will give precise results too.

Though, the results of the RM with different values of RD for both the empirical closed-form equations of the strut radius and the geometrical Equation (5) were compared with those of the ABAQUS diagnostic tool to show the accuracy of the former and the discrepancy of the latter as shown in Figure 23. Equation (5) given below is similar to other geometrical equations presented in the literature by several researchers.[26,27,56,57]

$$RD = \frac{V_{latt.}}{V_{sol.}} = \frac{4\pi R^2 \times \sqrt{X^2 + Y^2 + Z^2}}{X \times Y \times Z}. \quad (5)$$

As it can be seen from Figure 23, there is a good matching between the results of the empirical closed-form equations relating strut radius with RD and the ABAQUS diagnostic tool. While, Equation (5) shows a discrepancy in the results, which increases clearly with increasing the strut radius due to magnifying the error ensued from not considering properly the material overlapping at the strut joints when formulating the geometrical Equation (4) required to estimate

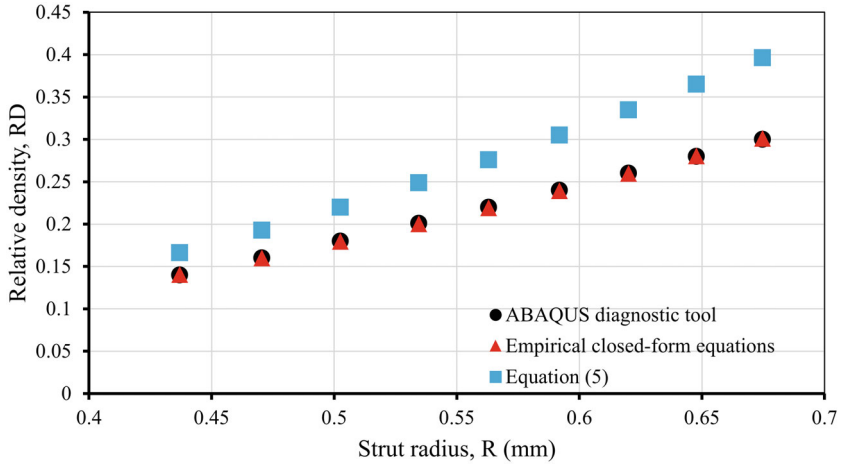

FIGURE 23 Comparing the results of the closed-form equations of the strut radius and the geometrical Equation (5) with those of ABAQUS diagnostic tool corresponding to the RM with different values of the RD.

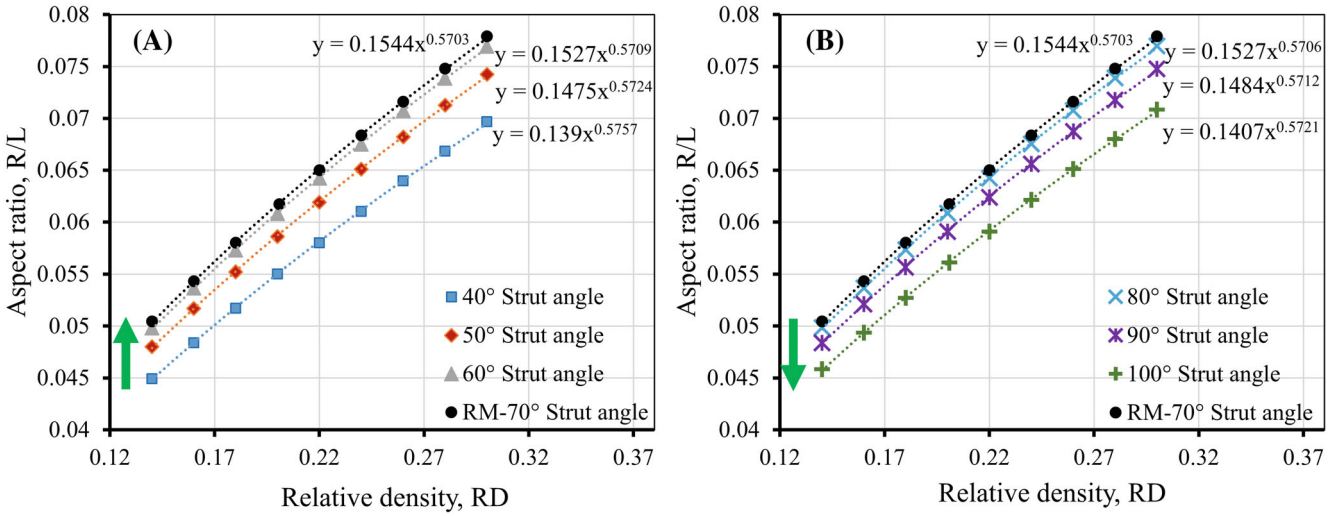

FIGURE 24 Empirical closed-form equations correlating aspect ratio with RD of FSLMs for strut angles (A) less and (B) higher than 70°

the actual lattice volume of the modified BCC LSs. In this regard, Equation (4) is considered an essential part of Equation (5), so any error embedded in Equation (4) will have an effect on the results of Equation (5). To this end, the empirical closed-form equations correlated with the strut radius with RD are really important in saving human time and effort. Because using them makes it possible to reduce the long procedure of the parametric study discussed earlier in Section 3, thereby enabling to determine directly and precisely the values of strut radius corresponding to any proposed RD.

5.3.3 | Aspect ratio of FSLMs and VSLMs

The aspect ratio (R/L) can be simply defined as a ratio of strut radius (R) to strut length (L). The latter is considered as a diagonal length measured from one edge to another of a single BCC lattice unit cell. Based on ABAQUS diagnostic tool, the strut lengths corresponding to each strut angle of all models in both sets were measured. Then, the strut radii were divided by the measured strut lengths to create the corresponding data of aspect ratio, which were thereafter correlated with RD to determine the empirical closed-form equations of the aspect ratio for both FSLMs and VSLMs as shown in Figures 24 and 25.

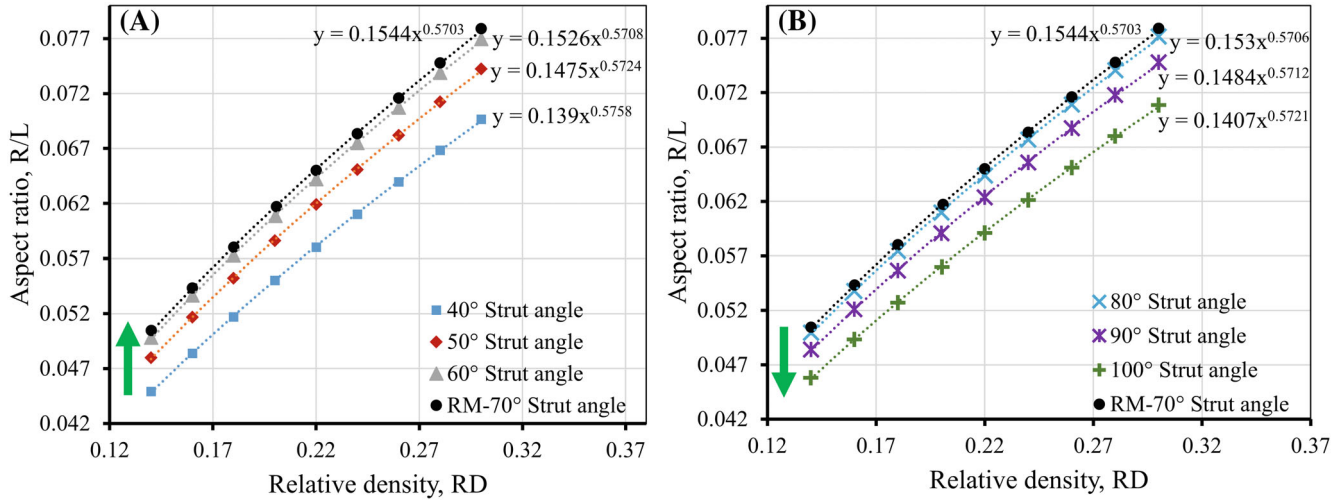

FIGURE 25 Empirical closed-form equations correlating aspect ratio with RD of VSLMs for strut angles (A) less and (B) higher than 70°

As it can be noticed, there is a power-function relationship between aspect ratio and RD with an exponent value around 0.57 for both FSLMs and VSLMs similar to the one ensued from the correlations of strut radius with RD. Indeed, this is reasonable since including the strut length in the empirical closed-form equations of strut radius will only have an effect on the values of the scaling factors while the exponent values do not change. In addition, the general trends of aspect ratio with strut angle variation for FSLMs are the same as those of the actual lattice volume and strut radius since the strut length is kept fixed for all FSLMs. However, the trends of aspect ratio with strut angle variation for VSLMs are different from those of actual lattice volume and strut radius. In other words, the actual lattice volume and strut radius trends of VSLMs with strut angle variation increase monotonically with increasing the strut angles. Whereas the trends of aspect ratio with strut angle variation increase with increasing the strut angles, strictly for strut angles lower than 70° as shown in Figure 25A and decrease with increasing the strut angles, only for strut angles higher than 70° as shown in Figure 25B. This is ascribed to the fact that VSLMs have variant strut lengths which increase with increasing the strut angles but do not vary through the layers of the same model corresponding to a specific strut angle. Significantly, even though the trends of strut radius with strut angle variation for VSLMs are different from those of FSLMs, the outcome of dividing the strut radius by the strut length makes the resultant trend of aspect ratio for VSLMs similar to FSLMs. This means that the scaling factors and exponent values of the empirical closed-form equations relating aspect ratio with RD for both VSLMs and FSLMs are identical. Up to this end, the aspect ratio of the empirical closed-form equations facilitates determining the strut length after estimating the strut radius, which is an essential step in estimating the dimensions of the lattice or overall lattice solid volume as it will be illustrated in the next section.

5.3.4 | Overall lattice solid volume of FSLMs and VSLMs

The overall lattice solid volume depends on the dimensions of a single unit cell (X, Y, and Z), which are related to the strut length (L) and angle (θ). After estimating the strut length from the previous section, these dimensions can be determined using Equations (6) and (7).

$$X = Z = \frac{0.7071L}{2\sqrt{\left(1+\left(\tan\left(\frac{\theta}{2}\right)\right)^2\right)}}, \tag{6}$$

$$Y = \frac{L \times \tan\left(\frac{\theta}{2}\right)}{2\sqrt{\left(1+\left(\tan\left(\frac{\theta}{2}\right)\right)^2\right)}}. \tag{7}$$

Therefore, the overall volume of a single unit cell and entire lattice can be estimated using Equation (8).

$$V_{sol.} = X \times Y \times Z \times N^3, \tag{8}$$

where N is the number of unit cells, assuming that the entire lattice has a cubic architecture or the same number of unit cells in all directions. As a backward step, the overall lattice solid volume will be used in estimating the RD.

5.4 | Generalization of the empirical closed-form equations

It is important to mention that all the empirical closed-form equations presented here to predict both the CMPs and GPs were developed based on $3 \times 3 \times 3$ lattice cell tessellation for the purpose of reducing the computational time as mentioned earlier in Section 4.5. That number of unit cells was selected after a preliminary investigation of the lattice cell tessellation effect on the elastic–plastic compressive mechanical behavior of the lattice (engineering stress–strain curve). Significantly, it has been found that a single unit cell offers higher CMPs, which decrease with increasing the number of unit cells. Besides, it has been observed that the general trends of the lattice mechanical response under compressive loading, that is, the resultant stress–strain curves, approached each other for lattice cell tessellations ($3 \times 3 \times 3$, $4 \times 4 \times 4$, and $5 \times 5 \times 5$) due to reducing the effect of boundaries. Based on that, it has been deduced that the empirical-closed form equations developed for predicting the values of the elastic modulus and yield stress of $3 \times 3 \times 3$ lattice cell arrangements can be employed to predict the same values, but for a higher number of unit cells including small error percentages. In addition, the effect of lattice cell tessellation was embedded in the empirical closed-form equations required to predict the actual volume occupied by the lattice and its dimensions to make them more general purpose. While there is no need to include that effect in the corresponding ones of the strut radius and aspect ratio since both are independent of the number of unit cells. In this regard, it is worthwhile mentioning that the empirical closed-form equations required to predict the GPs after including the effect of lattice cell tessellation are applicable for any unit cell number, that is, higher than or equal to $1 \times 1 \times 1$. In essence, corresponding to given values of RD, strut angle, and whether the type of modified BCC LSs is FSLM or VSLM. First, the elastic modulus, yield stress, and the associated mechanical properties can be predicted properly for unit cell numbers higher than or equal $3 \times 3 \times 3$ as explained in Figure 26.

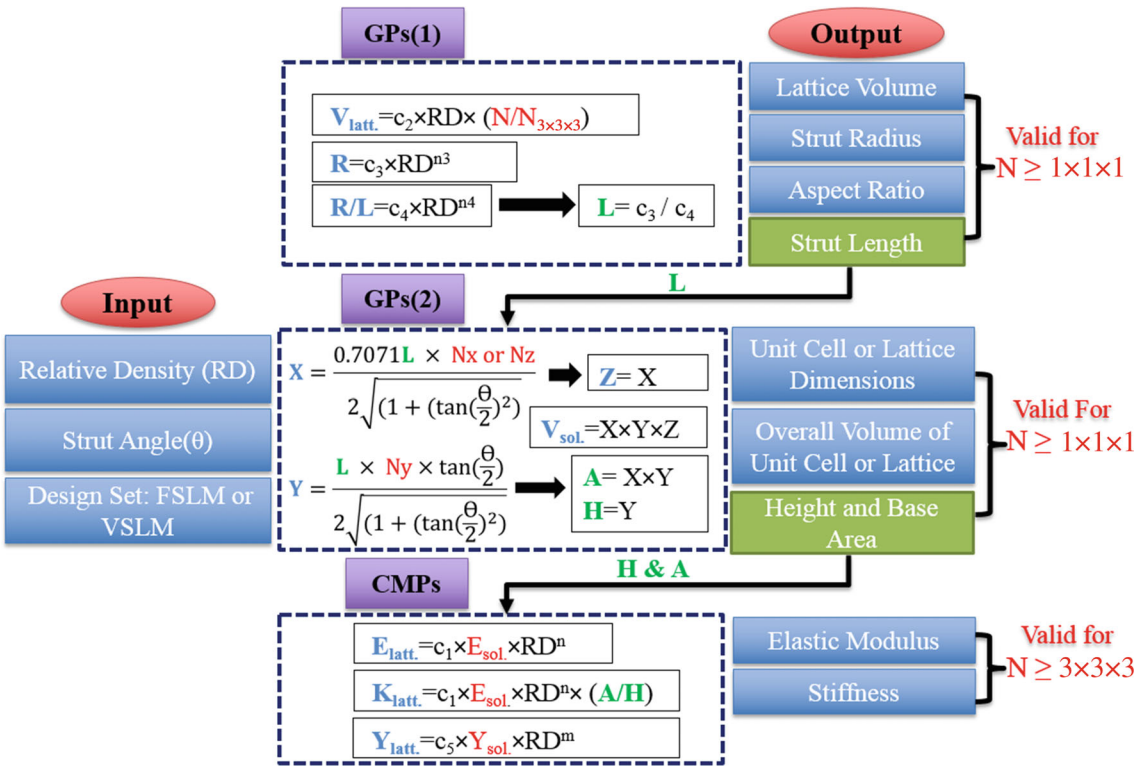

FIGURE 26 The logical sequence of the prediction process, starting with GPs and ending with CEMPs from top to bottom

Second, the GPs comprising the actual lattice volume, strut radius, aspect ratio, strut length, and the overall solid volume of the lattice or its dimensions can also be predicted well for any unit cell number as shown in Figure 26. To this end, it is clear to notice that there is a logical sequence in the prediction process as illustrated in Figure 26. It is starting from the top to bottom with the GPs (1) since the ensued strut length (L) is important in predicting the GPs (2). Then, the height (H) and the base area of the lattice (A) resultant from GP (2) are essential in predicting the CMPs.

6 | CONCLUSION

In the current research, generalized empirical closed-form equations were developed using scaling laws and FEMs in order to predict the CMPs and GPs of the modified BCC LSs based on strut length and orientation, including the effect of lattice cell tessellation and material distribution at strut joints. To achieve that goal, 117 models were built and analyzed with ABAQUS FE software. These models can be categorized based on the strut length as FSLMS and VSLMs. Each one has 63 lattice models distributed on seven strut angles (7), 40° to 100° with the step of 10°, and nine RDs (9), 0.14 to 0.3 with the step of 0.02, corresponding to each strut angle. As a design constraint applied to the FSLMs, the strut length is kept fixed through the layers of a certain model and fixed with strut angle variation from one model to another. Whereas in VSLMs, the strut length is varied with strut angle variation from one model to another. In addition, there are nine models corresponding to 70° strut angle duplicated in both sets called as RMs. For this reason, the total number of models adopted in this study is 117 models, not 126. After simulating the elastic–plastic compressive mechanical behavior of all lattice models and measuring their structural parameters, the data extracted from ABAQUS were fitted with Gibson and Ashby's scaling laws and correlated with RD to develop the empirical closed-form equations required to predict both the CMPs and the GPs.

It has been observed that the empirical closed-form equations can predict very well the CMPs of modified BCC LSs for $3 \times 3 \times 3$ unit cells. Also, it has been shown that these equations are still capable of predicting the CMPs for a higher number of unit cells with small error rates. This is done based on an investigation for the effect of the lattice cell tessellation on the elastic–plastic compressive mechanical performance of the modified BCC LSs. With including the number of unit cells as part of these equations, prediction of the GPs at a good level of accuracy has been demonstrated to be valid for any lattice cell repetitions using the empirical-closed form equations. Furthermore, it has been found that Gibson and Ashby's coefficients as well as the factors of aspect ratios are identical for both FSLMs and VSLMs. For this reason, the VSLMs of strut angles (40°, 50°, and 60°) are preferred over their counterparts of the FSLMS corresponding to the same values of RD since the actual lattice volumes or weight of the VSLMs are smaller or lighter than the corresponding ones of the FSLMs. However, the reverse occurs with strut angles higher than 70° where VSLMs are heavier than FSLMs, thereby making the latter preferable. Also, it has been noticed that the elastic modulus and yield stress increase with increasing the strut angles due to the tendency of the deformation mechanism to move toward stretch-dominated instead of bending with increasing the strut angles. The conclusion of this research can be summarized in two main points. First, the two lattice design sets with a variety of strut angles and RDs play a major role in space-based applications where the optimization of lattice volume or weight is of high significance. Second, the generalized empirical-closed form equations provide an efficient and straight-forward technique through which the CMPs and GPs can be varied or controlled by changing the RD. Indeed, this is a good way for giving the lattice designers a thorough insight into the elastic–plastic mechanical properties and structural parameters of a broader range of BCC LSs before starting the fabrication process. By that means, it will be possible to save more computational time, human efforts, and expenses required to conduct finite element simulation or experimental work.

To this end, it might be useful to mention that the current research focuses more on the computational techniques than the experimental work. Indeed, the manufacturing parameters (for example, layer thickness, in-fill density, building orientation) have influences on the mechanical characteristics of lattices.[58,59] In addition, the printed lattices are different from the ones that are designed and modeled using software. It usually includes some drawbacks, for instance residual stresses, struts' corrugations, high stress concentration at the strut nodes, and surface roughness, which in turn affect the lattice mechanics.[50,60,61] All these parameters and drawbacks were not considered in the current research. However, developing finite element models that could cover the manufacturing parameters and capture the real printed feature of lattices as well as could include gradient geometries will be a good topic for future study.

AUTHOR CONTRIBUTIONS

Hasanain S. Abdulhadi: Conceptualization (equal); formal analysis (lead); methodology (lead); validation (lead); writing – original draft (lead); writing – review and editing (equal). **Abdalsalam Fadeel:** Investigation (supporting); methodology (supporting); software (equal); validation (supporting); visualization (supporting); writing – review and editing (supporting). **Tahseen A. Alwattar:** Investigation (supporting); methodology (supporting); software (equal); validation (supporting); visualization (supporting); writing – original draft (supporting). **Ahsan Mian:** Conceptualization (equal); formal analysis (supporting); investigation (supporting); methodology (supporting); project administration (lead); resources (lead); supervision (lead); writing – review and editing (supporting).

CONFLICT OF INTEREST

The authors have no conflict of interest relevant to this article.

PEER REVIEW

The peer review history for this article is available at https://publons.com/publon/10.1002/eng2.12566.

DATA AVAILABILITY STATEMENT

The data that support the findings of this study are available from the corresponding author upon reasonable request.

ORCID

Hasanain S. Abdulhadi https://orcid.org/0000-0002-0702-5732
Ahsan Mian https://orcid.org/0000-0002-2033-6738

REFERENCES

1. Deshpande VS, Fleck NA, Ashby MF. Effective properties of the octet-truss lattice material. *J Mech Phys Solids*. 2001;49(8):1747-1769.
2. Deshpande VS, Ashby MF, Fleck NA. Foam topology bending versus stretching dominated architectures. *Compos Sci Technol*. 2003;63:2331-2343.
3. Deshpande VS, Fleck NA. Collapse of truss core sandwich beams in 3-point bending. *Int J Solids Struct*. 2001;38:6275-6305.
4. McKown S, Shen Y, Brookes WK, et al. The quasi-static and blast loading response of lattice structures. *Int J Impact Eng*. 2008;35(8):795-810.
5. Al Rifaie M, Abdulhadi H, Mian A. Advances in mechanical metamaterials for vibration isolation: a review. *Adv Mech Eng*. 2022;14(3):1-20.
6. Mellor S, Hao L, Zhang D. Additive manufacturing: a framework for implementation. *Int J Prod Econ*. 2014;149:194-201.
7. Gao W, Zhang Y, Ramanujan D, et al. The status, challenges, and future of additive manufacturing in engineering. *Comput Aided Des*. 2015;69:65-89.
8. Nguyen DS, Vignat F. A method to generate lattice structure for additive manufacturing. *IEEE*. 2016;2016:966-970.
9. Thompson MK, Moroni G, Vaneker T, et al. Design for Additive Manufacturing: trends, opportunities, considerations, and constraints. *CIRP Ann Manuf Technol*. 2016;65(2):737-760.
10. Gibson LJ, Ashby MF. *Celluar Solids: Structure and Properties, Cambridge*. Cambride University Press; 1997.
11. Ashby MF, Evans AG, Fleck NA, Gibson LJ, Hutchinson JW, Wadley HNG. *Metal Foams: A Design Guide, Woburn*. Butterworth-Heinemann; 2000.
12. Ashby MF. The properties of foams and lattices. *Philos Trans Royal Soc A*. 2006;364(1838):15-30.
13. Fadeel A, Abdulhadi H, Newaz G, Srinivasan R, Mian A. Computational investigation of the post-yielding behavior of 3D-printed polymer lattice structures. *J Comput Des Eng*. 2022;9(1):263-277.
14. Maskery I, Hussey A, Panesar A, et al. An investigation into reinforced and functionally graded lattice structures. *J Cell Plast*. 2017;53(2):151-165.
15. Zheng X, Lee H, Weisgraber TH, et al. Ultralight, ultrastiff mechanical metamaterials. *Am Assoc Adv Sci*. 2014;344(6190):1373-1377.
16. Maskery I, Sturm L, Aremu AO, et al. Insights into the mechanical properties of several triply periodic minimal surface lattice structures made by polymer additive manufacturing. *Polymer*. 2018;152:62-71.
17. Maskery I, Aremu AO, Parry L, Wildman RD, Tuck CJ, Ashcroft IA. Effective design and simulation of surface-based lattice structures featuring volume fraction and cell type grading. *Mater Des*. 2018;155:220-232.
18. Ahmadi SM, Yavari SA, Wauthle R, Schrooten J, Weinans H, Zadpoor AA. Additively manufactured open-cell porous biomaterials made from six different space-filling unit cells: the mechanical and morphological properties. *Materials*. 2015;8(4):1871-1896.
19. Ashby MF, Brechet YJ. Designing hybrid material. *Acta Mater*. 2003;51:5801-5821.
20. Smith M, Guan Z, Cantwell WJ. Finite element modelling of the compressive response of lattice structures manufactured using the selective laser melting technique. *Int J Mech Sci*. 2013;67:28-41.
21. Gümrük R, Karadeniz S, Mines R. Static mechanical behaviours of stainless steel micro-lattice structures under different loading conditions. *Mater Sci Eng A*. 2013;586:392-406.
22. Cetin E, Baykaso C. Energy absorption of thin-walled tubes enhanced by lattice structures. *Int J Mech Sci*. 2019;158:471-484.

23. Andani MT, Haberland C, Walker JM, et al. Achieving biocompatible stiffness in NiTi through additive manufacturing. *J Intell Mater Syst Struct*. 2016;27(19):2661-2671.
24. Zhu F, Lu G, Ruan D, Wang Z. Plastic deformation, failure and energy absorption of Sandwich structures with metallic cellular cores. *Int J Prot Struct*. 2010;1(4):507-541.
25. Karamooz Ravari MR, Andani MT. Prediction of the elastic response of TPMS cellular lattice structures using finite element method. Solid Freeform Fabrication Symposium; 2017:2060-2065.
26. Ushijima K, Cantwell W, Mines R, Tsopanos S, Smith M. An investigation into the compressive properties of stainless steel micro-lattice structures. *J Sandw Struct Mater*. 2010;13(3):303-329.
27. Ptochos E, Labeas G. Elastic modulus and Poisson's ratio determination of micro-lattice cellular structures by analytical, numerical and homogenisation methods. *J Sandw Struct Mater*. 2012;14(5):597-626.
28. Mines W. Compressive behaviour of stainless steel micro-lattice structures. *Int J Mech Sci*. 2013;68:125-139.
29. Alwattar TA, Mian A. Development of an elastic material model for BCC lattice cell structures using finite element analysis and neural networks approaches. *J Compos Sci*. 2019;3(2):33.
30. Fadeel A, Mian A, Al Rifaie M, Srinivasan R. Effect of vertical strut arrangements on compression characteristics of 3D printed polymer lattice structures: experimental and computational study. *J Mater Eng Perform*. 2018;28:709-716.
31. Bertolino G, Montemurro M. Two-scale topology optimisation of cellular materials under mixed boundary conditions. *Int J Mech Sci*. 2022;216:106961.
32. Montemurro M, Bertolino G, Roiné T. A general multi-scale topology optimisation method for lightweight lattice structures obtained through additive manufacturing technology. *Compos Struct*. 2021;258:113360.
33. Bertolino G, Montemurro M, Pasquale GD. Multi-scale shape optimisation of lattice structures: an evolutionary-based approach. *Int J Interact Des Manuf*. 2019;13(4):1565-1578.
34. Montemurro M, Refai K, Catapano A. Thermal design of graded architected cellular materials through a CAD-compatible topology optimisation method. *Compos Struct*. 2022;280:114862.
35. Al Rifaie MJ. *Resilience and Toughness Behavior of 3d-Printed Polymer Lattice Structures: Testing and Modeling*. MS Thesis. Wright State University; 2017.
36. Fadeel A, Abdulhadi H, Srinivasan R, Mian A. A computational approach in understanding the low-velocity impact behavior and damage of 3D-printed polymer lattice structures. *J Mater Eng Perform*. 2021;30:6511-6521.
37. Alwattar TA. *Developing Equivalent Solid Model for Lattice Cell Structure Using Numerical Approaches*. Ph.D. Wright State University; 2020.
38. Fadeel A. Development and Application of a Computational Modeling Scheme for Periodic Lattice Structure. Ph.D. Dissertation. Wright State University; 2021.
39. Parthasarathy J, Starly B, Raman S. A design for the additive manufacture of functionally graded porous structures with tailored mechanical properties for biomedical applications. *J Manuf Process*. 2011;13(2):160-170.
40. Beer FP, Johnston ER, DeWalf JT, Mazurek DF. *Mechanics of Material*. McGraw-Hill; 2015:1-823.
41. Habib FN, Iovenitti P, Masood SH, Nikzad M. Fabrication of polymeric lattice structures for optimum energy absorption using multi jet fusion technology. *Mater Des*. 2018;155(5):86-98.
42. Tadepalli SC, Erdemir A, Cavanagh PR. Comparison of hexahedral and tetrahedral elements in finite element analysis of the foot and footwear. *J Biomech*. 2011;44(12):2337-2343.
43. de Oliveira BL, Sundnes J. Comparison of tetrahedral and hexahedral meshes for finite element simulation of cardiac electro-mechanics. Proceedings of the VII European Congress on Computational Methods in Applied Sciences and Engineering (ECCOMAS Congress 2016); 2016:164-177.
44. Abdulhadi HS, Mian A. Effect of strut length and orientation on elastic mechanical response of modified body-centered cubic lattice structures. *J Mater Des Appl*. 2019;233:2219-2233.
45. Yang Y, Shan M, Zhao L, Qi D, Zhang J. Multiple strut-deformation patterns based analytical elastic modulus of sandwich BCC lattices. *Mater Des*. 2019;181:107916.
46. Abdulhadi HS. *Designing New Generations of BCC Lattice Structures and Developing scaling Laws to Predict Compressive Mechanical Characteristics and Geometrical Parametres*. Ph.D. Dissertation. Wright State Uinversity; 2020.
47. Kadkhodapour J, Montazerian H, Raeisi S. Investigating internal architecture effect in plastic deformation and failure for TPMS-based scaffolds using simulation methods and experimental procedure. *Mater Sci Eng C*. 2014;43:587-597.
48. Köhnen P, Haase C, Bültmann J, Ziegler S, Schleifenbaum JH, Bleck W. Mechanical properties and deformation behavior of additively manufactured lattice structures of stainless steel. *Mater Des*. 2018;145:205-217.
49. Egan PF, Gonella VC, Engensperger M, Ferguson SJ, Shea K. Computationally designed lattices with tuned properties for tissue engineering using 3D printing. *PLoS one*. 2017;12:1-20.
50. Yan C, Hao L, Hussein A, Young P. Ti – 6Al – 4V triply periodic minimal surface structures for bone implants fabricated via selective laser melting. *J Mech Behav Biomed Mater*. 2015;51:61-73.
51. Smith M, Cantwell WJ, Guan Z, et al. The quasi-static and blast response of steel lattice structures. *J Sandw Struct Mater*. 2011;13:479-501.
52. Leary M, Mazur M, Williams H, et al. Inconel 625 lattice structures manufactured by selective laser melting (SLM): mechanical properties, deformation and failure modes. *Mater Des*. 2018;157:179-199.
53. Mazur M, Leary M, Sun S, Vcelka M, Shidid D. Deformation and failure behaviour of Ti-6Al-4V lattice structures manufactured by selective laser melting (SLM). *Int J Adv Manuf Technol*. 2016;84:1391-1411.

54. Maconachie T, Leary M, Lozanovski B, et al. SLM lattice structures: properties, performance, applications and challenges. *Mater Des*. 2019;183:108-137.
55. Al-Saedi DS, Masood SH, Faizan-Ur-Rab M, Alomarah A, Ponnusamy P. Mechanical properties and energy absorption capability of functionally graded F2BCC lattice fabricated by SLM. *Mater Des*. 2018;144:32-44.
56. Ushijima K, Cantwell WJ, Chen DH. Estimation of the compressive and shear responses of three-dimensional micro-lattice structures. *Procedia Eng*. 2011;10:2441-2446.
57. Ushijima K, Cantwell WS, Chen DH. Prediction of the mechanical properties of micro-lattice structures subjected to multi-axial loading. *Int J Mechan Sci*. 2013;68:47-55.
58. Yadlapati SA. *Influenece of FDM Build Parameters on Tensile and Compression Behaviors of 3D Printed Polymer Lattice Structures*. MS Thesis. Wright State University; 2018.
59. Paul FE, Bauer I, Shea K, Ferguson SJ. Mechanics of three-dimensional printed lattices for biomedical devices. *J Mech Des*. 2019;141(3):031703.
60. Karamooz Ravari MR, Kadkhodaei M, Badrossama M, Rezaei R. Numerical investigation on mechanical properties of cellular lattice structures fabricated by fused deposition modeling. *Int J Mech Sci*. 2014;88:154-169.
61. Bai L, Yi C, Chen X, Su Y. Effective design of the graded strut of BCC lattice structure for improving mechanical properties. *Materials*. 2019;12(13):2192.

How to cite this article: Abdulhadi HS, Fadeel A, Alwattar TA, Mian A. Developing scaling laws to predict compressive mechanical properties and determine geometrical parameters of modified BCC lattice structures. *Engineering Reports*. 2022;e12566. doi: 10.1002/eng2.12566